JGR Space Physics

RESEARCH ARTICLE
10.1029/2020JA028943

Special Section:
Geospace multi-point observations in Van Allen Probes and Arase era

Relationship Between the Locations of the Midlatitude Trough and Plasmapause Using GNSS-TEC and Arase Satellite Observation Data

Atsuki Shinbori[1], Yuichi Otsuka[1], Takuya Tsugawa[2], Michi Nishioka[2], Atsushi Kumamoto[3], Fuminori Tsuchiya[4], Shoya Matsuda[5], Yoshiya Kasahara[6], and Ayako Matsuoka[7]

[1]Institute for Space-Earth Environmental Research, Nagoya University, Nagoya, Aichi, Japan, [2]National Institute of Information and Communications Technology, Koganei, Tokyo, Japan, [3]Department of Geophysics, Tohoku University, Sendai, Miyagi, Japan, [4]Planetary Plasma and Atmospheric Research Center, Tohoku University, Sendai, Miyagi, Japan, [5]Institute of Space and Astronautical Science, Japan Aerospace Exploration Agency, Sagamihara, Kanagawa, Japan, [6]Graduate School of Natural Science and Technology, Kanazawa University, Kanazawa, Japan, [7]Word Data Center for Geomagnetism, Graduate School of Science, Kyoto University, Kyoto, Japan

Abstract Relationship between the locations of the midlatitude trough minimum in the ionosphere and plasmapause in the inner magnetosphere has been statistically investigated using global navigation satellite system (GNSS)-total electron content (TEC) and electron density data obtained from the Arase satellite from March 23, 2017 to May 31, 2020. In this analysis, we identify the midlatitude trough minimum as a minimum value of GNSS-TEC at subauroral and midlatitude regions, and determine the plasmapause as an electron density decrease by a factor of 5 or more within $\Delta L < 0.5$ in the inner magnetosphere. As a result, the plasmapause does not always coincide with the midlatitude trough minimum in all magnetic local time (MLT) sectors under all geomagnetic conditions. During the geomagnetically quiet periods, the midlatitude trough minimum is located at higher and lower geomagnetic latitudes (GMLATs) of the plasmapause in the MLT ranges of 5–21 and 21–5 h, respectively. This implies that both the features could not be on the same magnetic field line. On the other hand, during the storm main phase, the midlatitude trough minimum and plasmapause move toward a low-latitude region with day-night and dawn-dusk asymmetries and the correlation becomes highest, compared with that under other geomagnetic conditions. Especially, both the features mapped on the ionosphere at a height of 300 km exist near GMLAT in the afternoon-midnight sectors. This suggests that the midlatitude trough and plasmapause are formed at almost the same location due to an enhanced subauroral polarization stream during the storm main phase.

Plain Language Summary The Earth's plasmasphere, which is filled with dense cold plasmas originating from the ionosphere, has a donut-like structure in the inner magnetosphere. The plasma density decreases gradually with an increasing distance from the topside ionosphere, and it decreases sharply around the plasmapause. The location of the plasmapause tends to move toward the Earth when the geomagnetic activity increases due to the arrival of solar wind disturbances to the magnetosphere. Furthermore, the plasmaspheric plasmas give major influence on plasma wave propagation, generation, absorption, and wave-particle interaction. Therefore, to investigate the shape of the plasmasphere and the spatial distribution of plasma density is important for understanding the generation processes of high-energetic particles in the inner magnetosphere. On the other hand, it has been thought that the midlatitude trough indicating the plasma density depletion in the ionosphere with a narrow latitudinal structure corresponds to the location of the plasmapause. In this study, we investigate the relationship between the locations of the midlatitude trough minimum in the ionosphere and plasmapause in the inner magnetosphere using global navigation satellite system-total electron content and electron density data obtained from the Arase satellite from March 23, 2017 to May 31, 2020.

Key Points:

- The midlatitude trough minimum do not always coincide with the plasmapause in all magnetic local time sectors under all geomagnetic conditions
- The correlation between the locations of the midlatitude trough minimum and plasmapause becomes highest during storm main phase
- The midlatitude trough minimum tends to be located near the plasmapause in the evening-midnight sectors during storm periods

Correspondence to:
A. Shinbori,
shinbori@isee.nagoya-u.ac.jp

Citation:
Shinbori, A., Otsuka, Y., Tsugawa, T., Nishioka, M., Kumamoto, A., Tsuchiya, F., et al. (2021). Relationship between the locations of the midlatitude trough and plasmapause using GNSS-TEC and Arase satellite observation data. *Journal of Geophysical Research: Space Physics*, *126*, e2020JA028943. https://doi.org/10.1029/2020JA028943

Received 20 NOV 2020
Accepted 6 APR 2021

1. Introduction

The midlatitude trough is characterized by a significant plasma depletion in the F-region of the ionosphere at subauroral and midlatitudes below the auroral oval. The structure of the midlatitude trough shows a

latitudinally narrow density depletion with a wide longitudinal extent. The midlatitude trough is frequently observed in the nighttime midlatitude ionosphere but extends from the afternoon to morning sectors (e.g., Aa et al., 2020; Chen et al., 2018; Kersley et al., 1997; Krankowski et al., 2009). The latitudinal structure of the midlatitude trough is divided into three parts: an equatorward wall, a trough minimum, and a poleward wall. The poleward wall has a sharp density gradient, where the electron density increases suddenly, and the equatorward wall shows a gradual increase of the electron density, which connects the normal low-latitude ionosphere (Muldrew, 1965; Werner & Prölss, 1997). Since the first identification of the midlatitude trough using the Allette satellite data (Muldrew, 1965), the midlatitude trough has been investigated with various kinds of instruments and techniques: ionosondes (Dudeney et al., 1983; Rothkaehl et al., 2000), incoherent scatter radars (Hedin et al., 2000; Ishida et al., 2014), global positioning system (GPS)–total electron content (TEC) observations (Holt et al., 1983; Krankowski et al., 2009; Shinbori et al., 2018; Zou et al., 2011, 2013), and low-Earth orbit satellite observations (Aa et al., 2020; Afonin et al., 1995; Chen et al., 2018; Karpachev et al., 2019; Yang et al., 2016, 2018).

Many statistical analysis and modeling studies have clarified several important features of the midlatitude trough: local time variation (Ahmed et al., 1979; Chen et al., 2018), seasonal and hemispheric variations (Aa et al., 2020), longitudinal variation during a geomagnetic storm (Shinbori et al., 2018) and solar cycle minimum (Chen et al., 2018), geomagnetic activity dependence (Yang et al., 2016), solar activity dependence (Yang et al., 2015), and interplanetary magnetic field (IMF) dependence (Voiculescu et al., 2006). The position of the midlatitude trough minimum occurs at higher latitude in the daytime and moves to the lower latitudes with late local times in the night and dawn sectors (Aa et al., 2020, Krankowski et al., 2009). The midlatitude trough usually moves to the lower latitudes with an increasing geomagnetic activity (Aa et al., 2020; Chen et al., 2018; Krankowski et al., 2009; Prölss, 2007; Shinbori et al., 2018; Yang et al., 2016; Zou et al., 2011). Yang et al. (2016) statistically investigated the position of the midlatitude trough as a function of the Dst index indicating the strength of geomagnetic storms, and found a rapid movement of the trough minimum to the pre-storm level within 20 h for moderate corotating interaction region (CIR) driven storms. Yang et al. (2016) also pointed out that the relationship between the positions of the midlatitude trough minimum and plasmapause breaks down during the recovery phase of geomagnetic storms.

As a formation process of the midlatitude trough, four types of generation mechanisms: flow stagnation, increasing recombination rate associated with increasing ion temperature, field-aligned plasma flow, and precipitation and transportation have been proposed by previous studies. In a case of the flow stagnation mechanism, the westward plasma flow associated with the westward dusk convection and eastward corotation flows with the Earth encounter each other at subauroral latitudes, and the plasma density decreases near the quasi-stagnation region due to long-time recombination in the dark region without photoionization (Spiro et al., 1978). This mechanism is thought as a candidate for the geomagnetically quiet-time midlatitude trough formation (Kelley, 2009; Nilsson et al., 2005). During geomagnetic storms and substorms, the intense poleward electric field related to a subauroral ion drift (SAID) (Spiro et al., 1979) or subauroral polarization stream (SAPS) (Foster & Burke, 2002) phenomenon appears at subauroral latitudes of the afternoon-midnight sectors. The westward fast plasma flow associated with the electric field increases the ion temperature due to ion-neutral frictional heating and enhances the nonlinear ion loss process (Rodger, 2008; Schunk et al., 1976). The enhanced frictional heating in the SAID/SAPS region and increasing ion-neutral relative velocity associated with meridional neutral wind cause field-aligned plasma flow which leads to the formation of the midlatitude trough (Anderson et al., 1991; Ishida et al., 2014). The poleward and equatorward walls of the midlatitude trough are thought to be formed by auroral particle precipitation and the replenishment of plasma from the nighttime plasmasphere, respectively (Rodger et al., 1986; Yizengaw & Moldwin, 2005). The high-density plasma transportation from the polar cap partially contributes to the formation of the poleward wall of the midlatitude trough (Rodger et al., 1986). Furthermore, the formation of a dayside trough can be related to the transportation of the nighttime decreased plasma into the daytime sector (Pryse et al., 1998; Rodger et al., 1992; Whalen, 1989).

On the other hand, the equatorial plasma density structure in the vertical direction above the F-region of the ionosphere shows a gradual decrease with an increasing L-value and the plasma density sharply decreases around $L = 4$–6. This boundary and the inner region with a high plasma density have been called the plasmapause and plasmasphere, respectively (Carpenter, 1966). The plasmapause is formed at the

location of counteraction of corotation and dawn-to-dusk convection electric fields in the magnetosphere (Nishida, 1966). Therefore, because the counteraction region moves toward the Earth with day-night and dawn-dusk asymmetries when the dawn-to-dusk convection electric field becomes strong, the plasmapause also moves toward the Earth during a significant enhancement of the convection electric field associated with geomagnetic disturbances such as a geomagnetic storm (e.g., Chappell et al., 1970; Oya & Ono, 1987; Shinbori et al., 2005). In this period, the region of high-dense plasma is formed in the magnetosphere of the noon-afternoon sectors beyond the plasmasphere, and this has been called plasmaspheric tail (Chappell, 1975) or plume (Ober et al., 1997). The global plasmaspheric observation by the IMAGE EUV (Inner Magnetopause to Aurora Global Experiment Extreme Ultraviolet Imager) instrument enables us to investigate temporal and spatial variations of the shape of the plasmasphere and plasmaspheric plume (e.g., Goldstein, 2004, 2006; Moldwin et al., 2016; Sandel et al., 2003). Foster et al. (2002) found that the storm-enhanced density (SED) plumes in the ionosphere are located on the same magnetic field line as the plasmaspheric plumes in the magnetosphere from a comparison between the GPS-TEC and IMAGE EUV observations during a large geomagnetic storm. Goldstein et al. (2005) proposed that the enhanced SAPS electric fields in addition to the convection electric field play a major role in the formation of the plasmaspheric plume and the erosion of the plasmasphere.

The relationship between the positions of the midlatitude trough and plasmapause has been investigated by many previous studies. Initial statistical analyses of the positions of the midlatitude trough have revealed that they are frequently observed on the same magnetic field lines as the plasmapause in the equatorial density distribution (e.g., Rycroft & Burnell, 1970; Rycroft & Thomas, 1970). Titheridge (1976) reported that the plasmapause projected onto the ionospheric height agrees with the midlatitude trough within approximately 2° of geomagnetic latitude (GMLAT) using the ALOUETTE 1 topside sounder data. Rodger et al. (1986) found that the poleward wall of the midlatitude trough is co-located at the plasmapause on the same magnetic field line in the evening-midnight sectors from the data analysis of the Advanced Ionospheric Sounder at Halley and the Dynamics Explorer-2 satellite. Using ground whistler and ionosonde observations, Rodger and Pinnock (1982) and Smith et al. (1987) showed that the plasmapause and the midlatitude trough often appear on the same magnetic field line, and that two features are closely co-located in the morning sector but separated with a distance of up to $L = 2$ in the evening sector. However, since most of the above previous studies identified the location of the plasmapause with an indirect method, direct comparison between the locations of the plasmapause and midlatitude trough has not been conducted. Yizengaw and Moldwin (2005) identified the plasmapause and midlatitude trough using IMAGE EUV images and GPS TEC data in the European and Australian sectors, and concluded that the plasmapause in the inner magnetosphere closely connects the midlatitude trough in the ionosphere on the same magnetic field line. Furthermore, Yizengaw et al. (2005) confirmed that a local time distribution of the plasmapause has high correlation with that of the midlatitude trough from 40 simultaneous observations of IMAGE EUV images and global ionospheric maps of TEC with 1-h interval. They also showed that the plasmapause tends to lie equatorward of the midlatitude trough in the daytime during both geomagnetically disturbed and quiet periods. Recently, Shinbori et al. (2018) also reported that the location of the plasmapause almost agrees with that of the midlatitude trough minimum during a geomagnetic storm that occurred on April 4, 2017 from a comparison between the electron density in the inner magnetosphere obtained from the Arase satellite and global navigation satellite system (GNSS)-TEC observations. From the long-term data analysis of the DEMETER (Detection of Electro-Magnetic Emissions Transmitted from Earthquake Regions) satellite observation, Chen et al. (2018) showed that the plasmapause lies equatorward of the midlatitude trough minimum in all geographic longitudes and that both the positions have a significant longitudinal variation. They also pointed out that the position of the plasmapause is less sensitive to the geomagnetic activity than that of the midlatitude trough. Thus, because most of the studies used several remote sensing data (e.g., EUV images and lightning whistler observations) for identification of the plasmapause in the inner magnetosphere, there is a possibility that the location of the plasmapause is different from that obtained from in situ observations in the inner magnetosphere. Moreover, it remains unknown how different the relationship between the plasmapause and midlatitude trough locations is during geomagnetically quiet times, main and recovery phases of geomagnetic storms.

In this study, we investigate long-term observation data of global GNSS-TEC and electron density in the inner magnetosphere obtained from the Arase satellite with high time and spatial resolutions and clarify the

relationship between the locations of the plasmapause and midlatitude trough minimum during geomagnetically quiet times, main and recovery phases of geomagnetic storms.

2. Observation Data and Analysis Method

2.1. Datasets

We use 1-min high resolution OMNI (HRO) data of the B_y and B_z components of the IMF in geocentric solar magnetic coordinates, solar wind proton density, and flow speed and geomagnetic indexes (auroral electrojet [AE] and horizontal symmetric disturbance [SYM-H]). The OMNI data are provided by the National Aeronautics and Space Administration (NASA) Coordinated Data Analysis Web (CDAWeb) (https://cdaweb.sci.gsfc.nasa.gov/index.html/). The AE index (World Data Center for Geomagnetism, Kyoto et al., 2015) and the SYM-H index (Iyemori, 1990; Iyemori & Rao, 1996) are provided by the World Data Center for Geomagnetism, Kyoto University (http://wdc.kugi.kyoto-u.ac.jp/index.html). For identification of geomagnetically quiet days, we refer to a list of geomagnetically quiet and disturbed days provided by the GFZ German Research Centre for Geosciences (https://www.gfz-potsdam.de/Kp-index/).

The two-dimensional (2D) GNSS-TEC data used for this analysis are derived from GNSS data in receiver independent exchange (RINEX) format obtained from many regional GNSS receiver networks all over the world. The number of GNSS stations reached more than 9,000 in January 2020. These RINEX files were provided by 50 data providers that have been listed on the GNSS-TEC website at Nagoya University (http://stdb2.isee.nagoya-u.ac.jp/GPS/GPS-TEC/gnss_provider_list.html).

We also use electric potential map data from midlatitude to high latitude calculated with the SuperDARN Assimilative Mapping (SAM) procedure (Cousins et al., 2013) to investigate the temporal and spatial variations of high-latitude plasma convection for solar wind and IMF conditions. The electric potential data and analysis software are provided by Virginia Tech (http://vt.superdarn.org/tiki-index.php?page=ASCIIData). Details of midlatitude SuperDARN and several science topics have been described in a review study by Nishitani et al. (2019).

The Arase satellite was launched at 11:00 (UT) on December 20, 2016 from Uchinoura Space Center and started full-operation observations after March 24, 2017. The satellite orbit is a geo-transfer orbit having an inclination of 31°, initial apogee and perigee of 32,000 and 400 km, respectively. The orbital period is 570 min (Miyoshi, Shinohara, et al., 2018). From the characteristics of the Arase satellite orbit, we can see electromagnetic and particle environments in the inner magnetosphere covering a wide L-shell range of up to 10–11. In this study, we use plasma wave dynamic spectrum data in a frequency range from 3 kHz to 10 MHz obtained from High Frequency Analyzer (HFA) (Kumamoto et al., 2018), which is a subcomponent of the Plasma Wave Experiment (PWE) (Kasahara, Kasaba, et al., 2018) onboard the Arase satellite, to derive the electron density from the upper limit frequency of upper hybrid resonance (UHR) waves. In this analysis, we use the electric field spectrum data of plasma waves with time resolution of 1 or 8 s. We also use magnetic field data along the Arase satellite orbit obtained from the MGF instrument (Matsuoka, Teramoto, Nomura, et al., 2018) when we calculate the electron density in the inner magnetosphere from the upper limit frequency of UHR waves. The Common Data Format (CDF) data of the HFA plasma wave spectrum and magnetic field are provided by ERG Science Center, Nagoya University (https://ergsc.isee.nagoya-u.ac.jp/data_info/index.shtml.en) (Miyoshi, Hori, et al., 2018).

2.2. Analysis Method

In this study, we calculate the GNSS-TEC value with a time resolution of 30 s from the collected GNSS data according to the procedure described in two studies by Sori et al. (2019) and Shinbori et al. (2020). Because the calculated relative TEC value has the instrumental biases, the estimation of them is required to derive the absolute TEC value. For estimation of the instrumental bias, we applied the method proposed by Otsuka et al. (2002). This method estimates 1-h average TEC and inter-frequency biases by weighted least squares fitting of the relative TEC value for each GNSS station and excludes the biases from the relative TEC values. Detailed description of the estimation of the absolute TEC value can be found in Otsuka et al. (2002).

Further, we calculate the vertical TEC value from the slant value and map it onto the thin shell ionosphere at an altitude of 300 km. In this method, we set the maximum satellite zenith angle to 75° when we create grid data of the absolute TEC. The time and spatial resolution of the data are 30 s and 0.5° × 0.5° in longitude and latitude, respectively. We also convert the smoothed TEC data with pixel smoothing with a boxcar window of 2.5° × 2.5° in geographic latitude and longitude every 5 min into netCDF-formatted data to easily deal with the TEC data using Space Physics Environment Data Analysis System (SPEDAS; Angelopoulos et al., 2019) and Inter-university Upper atmosphere Observation NETwork (IUGONET; Hayashi et al., 2013) data analysis software (UDAS; Tanaka et al., 2013). These GNSS-TEC data are stored in a database (http://stdb2.isee.nagoya-u.ac.jp/GPS/GPS-TEC/) managed by the PWING (study of dynamical variation of Particles and Waves in the INner magnetosphere using Ground-based network observations) project (Shiokawa et al., 2018).

Because the spatial distribution of the electron density in the ionosphere changes as a function of geographic latitude and longitude and local time, the absolute TEC value also varies, depending on these parameters. Therefore, we need to exclude the average TEC value during the geomagnetically quiet periods to magnify the signature of midlatitude trough associated with geomagnetic storms and substorms. In this analysis, we use the normalized TEC difference as the ratio of the TEC difference (rTEC) introduced by Sori et al. (2019) and Shinbori et al. (2020). The rTEC value can be obtained by normalizing the TEC difference between the TEC value every day and average quiet-day TEC value using the absolute value of the average TEC. When we calculate the average quiet-day TEC value, we select the TEC values during 10 geomagnetically quiet days per month using a list of quiet and disturbed days. Finally, we create 2D polar maps of the TEC and rTEC in geographic and geomagnetic coordinates, respectively, and a GMLAT-time plot (keogram) of the TEC and rTEC along the geomagnetic longitude of the Arase satellite position projected onto the ionosphere at a height of 300 km with Tsyganenko 04 magnetic field model (Tsyganenko & Sitnov, 2005). In this keogram, we determine a minimum value of rTEC or TEC in a lower latitude region of an enhancement of rTEC or TEC associated with an auroral oval as a midlatitude trough minimum. We also use the Altitude-Adjusted Corrected Geomagnetic Model (AACGM) (Shepherd, 2014) for transformation from geographic coordinates to geomagnetic coordinates, and overplot the contours of SuperDARN electric potential from subauroral to high latitudes on the polar maps of the TEC and rTEC.

To obtain the electron density distribution in the inner magnetosphere on the Arase satellite orbit, we first identify the upper limit frequency of the UHR waves in the plasma wave dynamic spectra obtained from the Arase PWE-HFA instrument. The frequency is plotted with a pink line in the dynamic spectra shown in Figure 1a. The upper limit frequency f_{UHR} is written by Equation 1

$$f_{UHR} = \sqrt{f_{pe}^2 + f_{ce}^2} \tag{1}$$

where the parameters f_{pe} and f_{ce} are electron plasma and cryotron frequencies, respectively. Because these frequencies are given by Equations 2 and 3

$$f_{pe} = \frac{1}{2\pi}\sqrt{\frac{e^2 n}{\varepsilon_0 m_e}} \tag{2}$$

$$f_{ce} = \frac{1}{2\pi}\frac{eB}{m_e} \tag{3}$$

where the parameters e, n, m_e, ε_0, and B are electron charge, density, mass, permittivity in vacuum, and magnetic field intensity, respectively, we can obtain the electron density from the electron plasma frequency. In this calculation, we use the magnetic field intensity obtained from the MGF instrument onboard the Arase satellite. Figure 1b shows the electron density in a region from the ionosphere to the inner magnetosphere on November 7, 2017 obtained from the above method. We further determine the plasmapause with a definition by Carpenter and Anderson (1992), who selected an electron density depression by a factor of 5 or more within $\Delta L < 0.5$ as a plasmapause phenomenon. The plasmapause position determined by this definition is shown by a red arrow in Figure 1b.

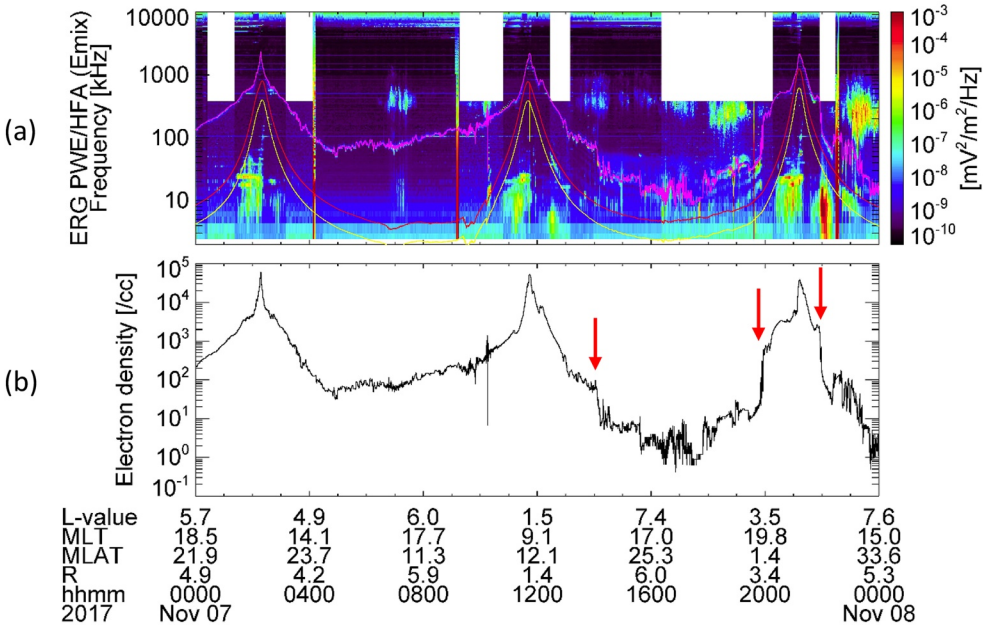

Figure 1. (a) Dynamic spectra of plasma waves in a frequency range from 3 kHz to 10 MHz obtained from the PWE-HFA instrument onboard the Arase satellite and (b) electron density in the inner magnetosphere at the Arase satellite derived from the upper limit frequency of the UHR waves on November 7, 2017. The pink, red, and yellow curves in (a) indicate the upper limit frequency of the UHR waves, the electron cyclotron frequency, and half electron cyclotron frequency, respectively. The red arrows in (b) show the location of the plasmapause determined from the definition of Carpenter and Anderson (1992). HFA, High Frequency Analyzer; PWE, Plasma Wave Experiment; UHR, upper hybrid resonance.

3. Temporal and Spatial Variation of the Electron Density in the Ionosphere and Magnetosphere During a Geomagnetic Storm on November 7–8, 2017

Figure 2 shows a time-series plot of (a) IMF B_y, (b) IMF B_z, (c) solar wind proton density, (d) solar wind flow speed, (e) AE index, and (f) SYM-H index from November 6 to 10, 2017. In Figure 2c, the solar wind proton density began to gradually increase after 18:00 UT on November 6 and reached the maximum value of 57.2 [/cc] at 04:33 UT on November 7. After that, the solar wind proton density decreased to a level before the start time of the proton density enhancement. In Figure 2d, the solar wind flow speed began to gradually increase from 305 to 651 [km/s] at 02:22 UT on November 7 after the onset of an increase of solar wind proton density. The pattern of solar wind proton density and flow speed variations is categorized into CIRs (Heber et al., 1999). In Figures 2a and 2b, the B_y and B_z components of the IMF showed larger fluctuations with their peak-to-peak amplitude of ∼20 nT on 7 November after the enhancement of solar wind flow speed. The B_z component was directed southward many times as seen in Figure 2b. In Figure 2f, the SYM-H index showed a significant decrease up to −89 nT after the enhancement of the solar wind flow speed and negative B_z component of the IMF. This signature of the SYM-H index indicates that a ring current develops in the inner magnetosphere (Iyemori, 1990). In Figure 2e, the AE index also showed a large enhancement associated with an increasing auroral activity at high latitudes after the onset of this geomagnetic storm.

Figure 3 shows 2D polar maps of rTEC in the Northern Hemisphere in geomagnetic coordinates. The thick and thin black lines show day-night terminators at a height of 105 and 300 km, respectively. The contour lines at high latitudes represent the electric potential derived from the SuperDARN radar observations. The color code indicates the rTEC value in a range of ±1.0. The red dashed lines indicate the location of midlatitude trough minimum. During a pre-storm phase (Figure 3a), the enhanced rTEC region with the rTEC value of more than 1.0 was confined at a GMLAT of more than 70°. The decreased rTEC region indicating the midlatitude trough appeared at a lower latitude of the enhanced rTEC region. The size of the two-cell convection indicated by the electric potential contour also become small. During a main phase of the geomagnetic storm (Figures 3b–3e), the enhanced rTEC region indicating a latitudinally narrow structure appeared

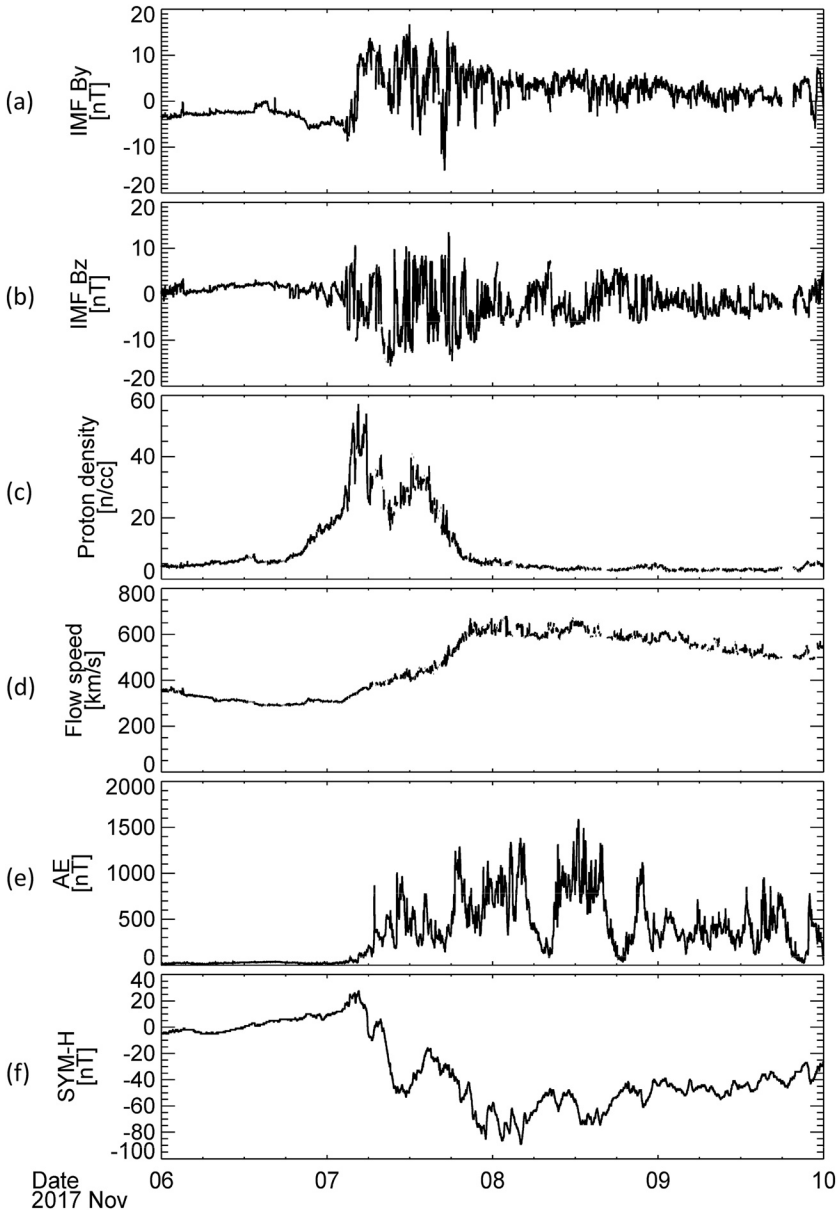

Figure 2. (a) IMF B_y, (b) IMF B_z, (c) solar wind proton density, (d) solar wind flow speed, (e) AE index, and (f) SYM-H index during November 6–10, 2017. AE, auroral electrojet; IMF, interplanetary magnetic field.

at a lower latitude of the center of the two-cell convection in association with storm-time auroral activity. The decreased rTEC region also appeared with a latitudinally narrow structure equatorward of the enhanced rTEC region. These rTEC structures moved to the lower latitude, corresponding to the low-latitude expansion of the two-cell convection. In Figure 3e, the electric potential contour in the dusk convection cell become denser along the midlatitude trough structure in the afternoon-premidnight sectors. This potential structure is due to the SAPS electric field which is formed during the main phase of the geomagnetic storm. In Figures 3c–3e, other rTEC enhancements related to the midlatitude broad SED and SED plume (e.g., Coster et al., 2017) can be seen in the midlatitude to low-latitude regions of the noon-evening sectors at the lower latitude of the midlatitude trough. During a recovery phase of the geomagnetic storm (Figures 3f–3h), the enhanced rTEC structure related to the auroral activity and SED phenomena decayed with time, and the size of the two-cell convection also become small. However, the decreased rTEC structure related to the midlatitude trough can be clearly seen in the subauroral latitude and midlatitude regions (e.g., Figure 3h).

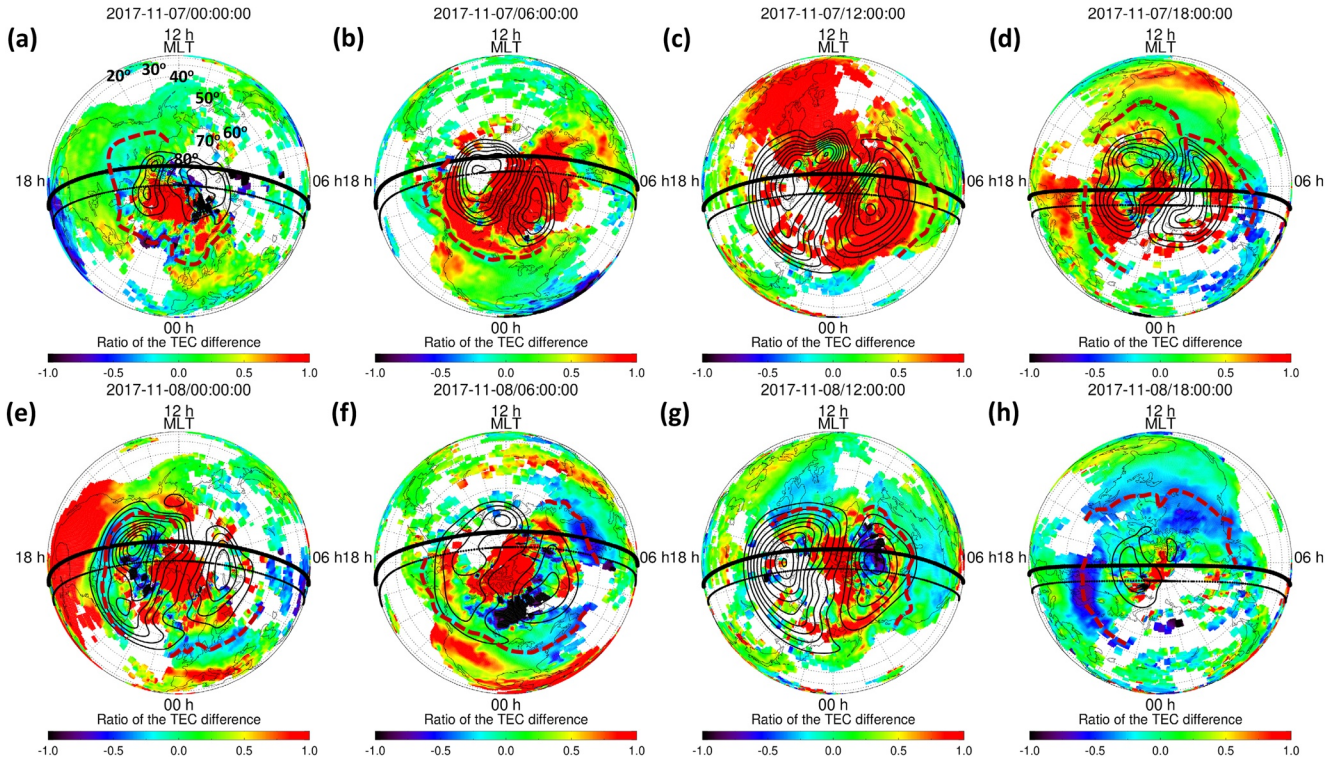

Figure 3. Two-dimensional polar maps of rTEC in geomagnetic coordinates. The thick and thin curves in the rTEC maps show day-night terminators at a height of 105 and 300 km, respectively. The line contours in each polar map give the electric potential at high latitudes calculated with the SuperDARN radar observations. The red dashed lines indicate the location of the midlatitude trough minimum. TEC, total electron content.

Figure 4 shows the orbit of the Arase satellite in the (a) *X-Y* and (b) *Y-Z* planes in solar magnetic (SM) coordinates in the same time interval of L-t plot in Figure 5. Because the Arase satellite traversed in the same direction as the Earth's rotation, the in-bound and out-bound passes covered the morning-evening and evening-postmidnight sectors, respectively. In this case, we can investigate a day-night difference in the response of the electron density structure in the inner magnetosphere to the geomagnetic storm. Figure 5 shows a time-series plot of (a) IMF B_z, (b) SYM-H index, (c–d) L-t diagrams of the electron density in the inner magnetosphere, and (e–f) plasmapause position for the in-bound and out-bound passes during November 5–15, 2017. In the in-bound pass (Figure 5c), the electron density began to decrease in an *L*-value range from 3.0 to 9.0 approximately 12 h after the onset of the main phase of the geomagnetic storm. In the outer region of $L > 5.0$, the electron density decreased up to less than 1.0 [/cc] during the main and early recovery phases. After that, the electron density gradually increased with time, and recovered a geomagnetically

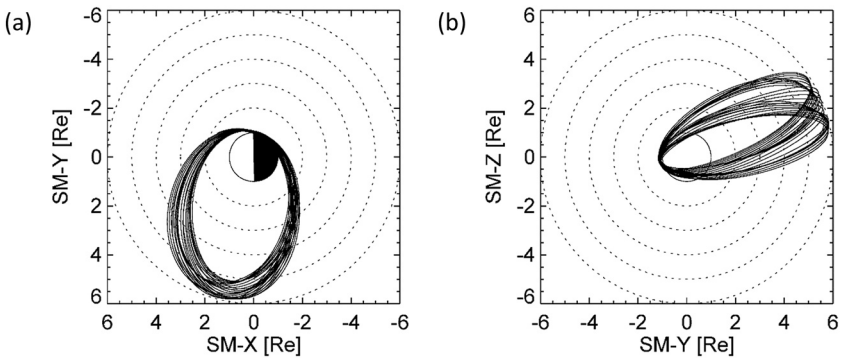

Figure 4. Arase satellite orbit on the *X-Y* and *Y-Z* plane planes in solar magnetic (SM) coordinates during November 5–15, 2017.

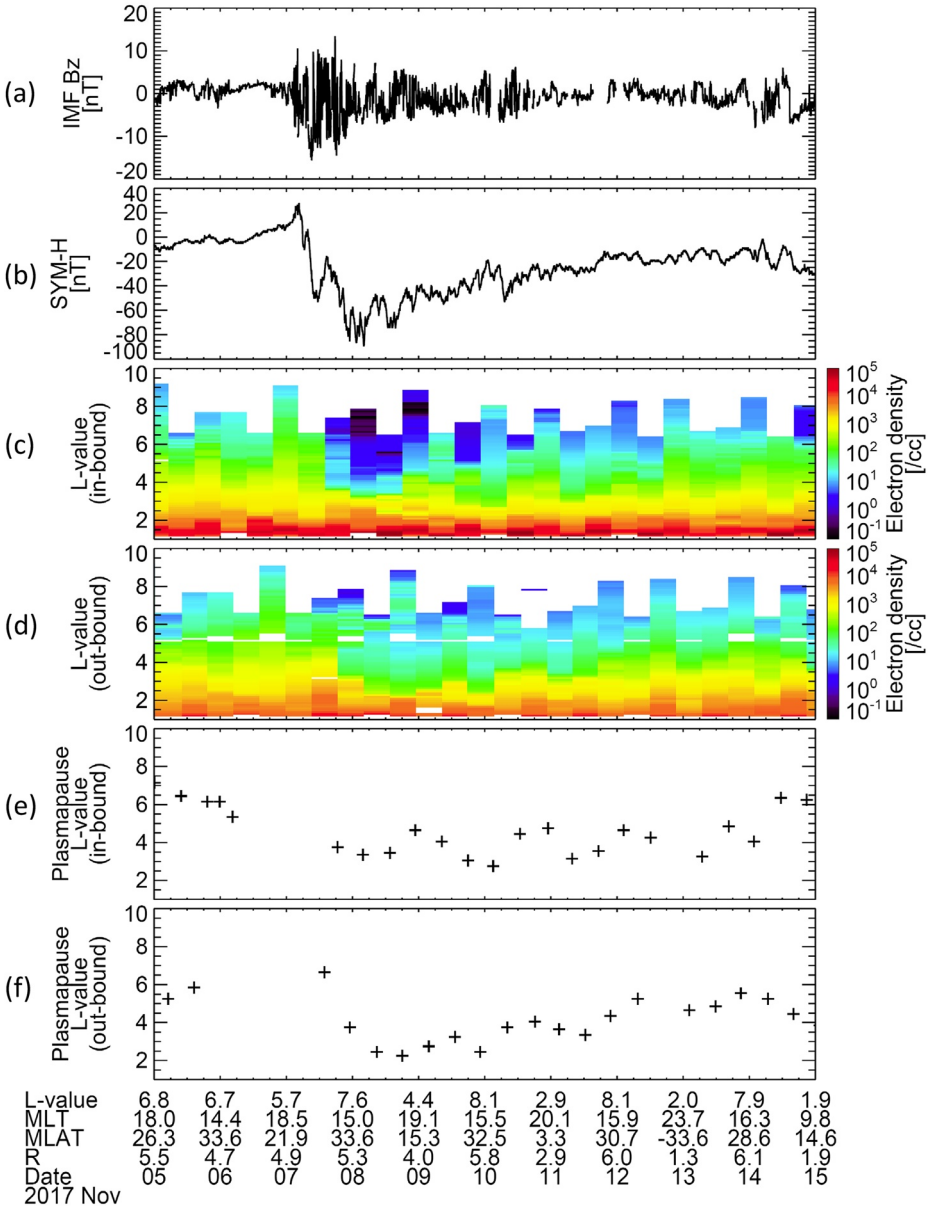

Figure 5. (a) IMF B_z, (b) SYM-H, (c and d) L-t diagrams of electron density in the inner magnetosphere for the in-bound and out-bound passes of the Arase satellite, (e and f) location of the plasmapause during November 5–15, 2017. The electron density indicated the color code in a range from 10^{-1} to 10^{5} [/cc]. IMF, interplanetary magnetic field.

quiet level approximately 5 days after the onset of the recovery phase. Also in the out-band pass, the electron density tended to decrease during the main phase, but the decreased level at $L > 4.0$ was smaller than that in the in-bound pass. Further, the region having an electron density of more than 500 [/cc] was more shrunk toward the Earth in the out-band pass, compared with that in the in-bound pass. In Figures 5e and 5f, the plasmapause position moved toward the Earth in both the in-bound and out-bound passes during the main and early recovery phases. The plasmapause in the out-bound pass tended to be located at a lower L-value than that in the in-bound pass. During the recovery phase after November 9, the plasmapause gradually moved away the Earth with several inward motions. From this analysis of the electron density in the inner magnetosphere, it is shown that the response of the electron density to the geomagnetic storm was different from different magnetic local time (MLT) sectors.

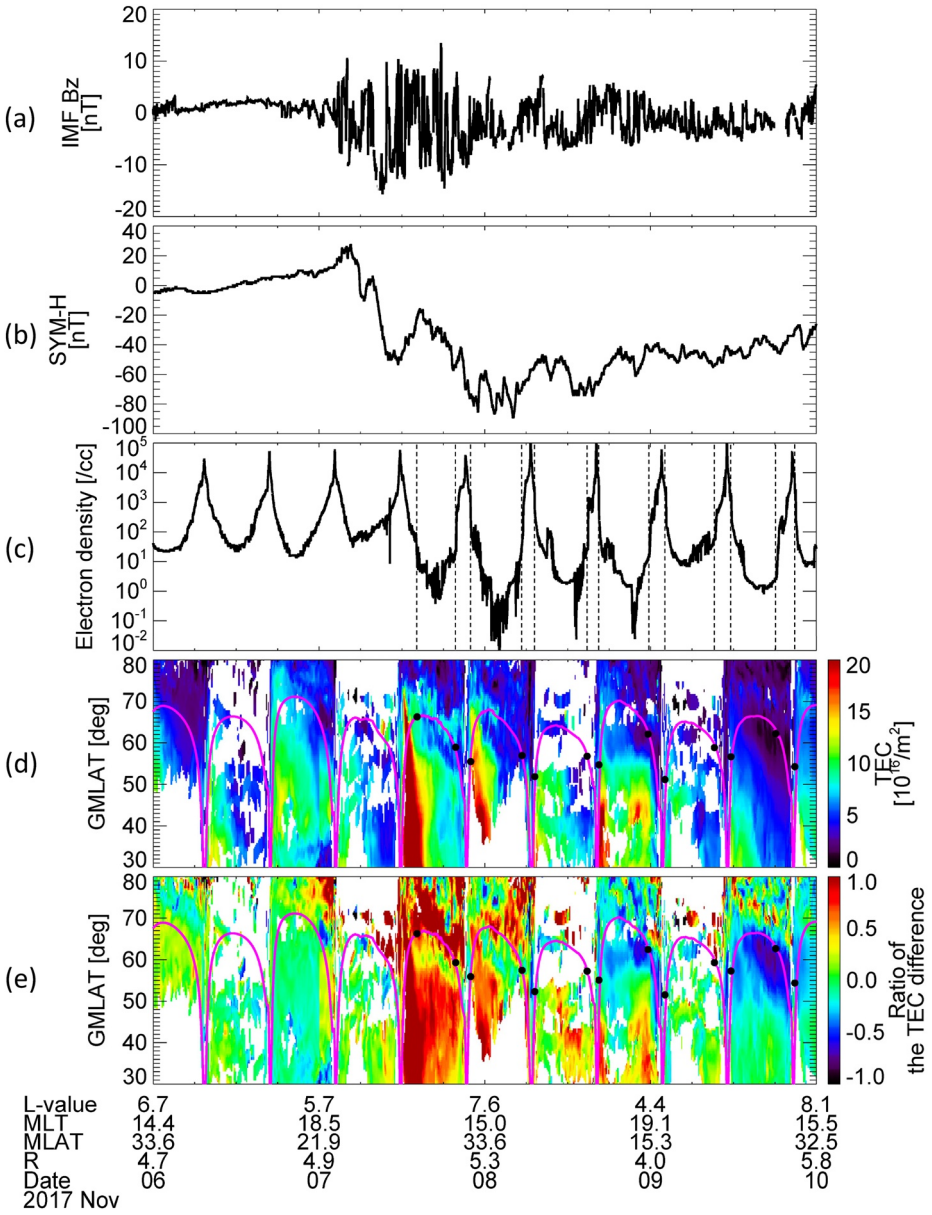

Figure 6. (a) IMF B_z, (b) SYM-H, (c) electron density, (d) and (e) geomagnetic latitude-time plots (keograms) of TEC and rTEC during November 6–10, 2017. The TEC and rTEC values indicate the color codes from 0 to 10 in TEC unit [10^{16}/m^2] and from −0.8 to 0.8, respectively. The variceal lines in (c) show the location of the plasmapause. The pink curves in (d and e) are the footprint of the Arase satellite orbit projected at a height of 300 km in the ionosphere with the Tsyganenko 04 magnetic field model. The black circles in (d and e) give the location of the plasmapause at a height of 300 km. IMF, interplanetary magnetic field.

To investigate the relationship between the location of the midlatitude trough minimum and the plasmapause, we created a GMLAT-time plot (keogram) of TEC and rTEC at the footprint of the Arase satellite. Figure 6 shows a time-series plot of (a) IMF B_z, (b) SYM-H index, (c) electron density, (d) and (e) keograms of TEC and rTEC during November 6–10, 2017. The vertical dashed lines in Figure 6c are the location of the plasmapause. The pink curves in Figures 6d and 6e indicate the footprint of the Arase satellite at a height of 300 km. The black circles on the pink curves give the location of the plasmapause corresponding to the dashed lines in Figure 6c. As already described in Figure 5, because the plasmapause moved to a lower L-value after the onset of the main phase of the geomagnetic storm, the location of the plasmapause moved to a lower latitude from 67° to 53°, and gradually moved to a poleward region during the recovery phase.

The midlatitude trough with a latitudinally narrow TEC or rTEC depletion clearly appeared in a latitudinal range from 50° to 70°, and the location moved to a lower latitude after the onset of the main phase of the geomagnetic storm. Compared with the location of the plasmapause, it tended to appear near the structure of the midlatitude trough but did not always coincide with an equatorial wall of the midlatitude trough as shown in previous studies (e.g., Figure 3 reported by Chen et al. [2018]).

4. Statistical View of the Relationship Between the Locations of the Midlatitude Trough Minimum and Plasmapause Under Different Geomagnetic Conditions

In Section 3, we showed that the locations of the midlatitude trough minimum and plasmapause tended to move toward the lower GMLAT and Earth, respectively, after the onset of the main phase of the geomagnetic storm that occurred on November 7–8, 2017. The location of the plasmapause projected at a height of 300 km in the ionosphere did not always coincide with an equatorward wall of the midlatitude trough, which is different from the results shown in previous studies (e.g., Chen et al., 2018; Yizengaw et al., 2005). In this section, we show the statistical analysis result of the relationship between the locations of the midlatitude trough minimum and plasmapause during geomagnetically quiet days, main and recovery phases of the geomagnetic storms in a period of about 3 years (March 22, 2017 to May 31, 2020). In this case, we analyzed 7,218 simultaneous events of the midlatitude trough minimum and plasmapause identified from the GNSS-TEC and Arase satellite observations. Of these events, we identified 2,079, 402, and 1,142 events during geomagnetically quiet days, main, and recovery phases of the geomagnetic storms, respectively. In this analysis, we selected a depletion of the SYM-H index with the minimum value of less than −30 nT as a geomagnetic storm.

Figure 7 shows the correlation between the locations of the midlatitude trough minimum and plasmapause for (a) all events, (b) geomagnetically quiet days, (c) storm main phase, and (d) storm recovery phase. In this figure, a common feature among all cases shows a positive correlation between the locations of the midlatitude trough minimum and plasmapause; that is, as the midlatitude trough minimum moves equatorward, the plasmapause at the ionospheric height moves to the lower latitude. The correlation coefficient becomes highest for the main phase of the geomagnetic storms while it becomes lowest for the geomagnetically quiet days. In Figure 7b, most of the geomagnetically quiet day events concentrate on the higher latitude (60°–70°: plasmapause, 55°–75°: midlatitude trough minimum), compared with those during the disturbed periods. During the geomagnetic storms, the lower limit of the GMLAT of the midlatitude trough minimum and plasmapause reaches up to 40°.

Figure 8 shows a MLT variation of the midlatitude trough minimum and plasmapause for (a) all events, (b) geomagnetically quiet days, (c) storm main phase, and (d) storm recovery phase. The black and red lines indicate the median values of the plasmapause and midlatitude trough minimum locations every hour in the MLT window of ±1.0 h, respectively. The error bars of each curve mean the standard error of the median values. In this case, the standard error E is derived from the following equation with a mean deviation D of the median values,

$$E = \frac{1}{n-1} * 1.96 * T$$
$$D = \frac{1}{n}\sum_{i=1}^{n}\left|x_i - m\right|$$

where n is the number of data, x_i each value, and m median value, respectively. During the geomagnetically quiet days (Figure 8b), the plasmapause was located at a GMLAT of 65°–67° with a small MLT variation while the midlatitude trough minimum had a clear MLT variation, indicating that the location moved to a lower latitude in the night time sector. The maximum and minimum values of the GMLAT were 69.5° at 12 h and 63.3° at 2 h (MLT), respectively. Furthermore, the midlatitude trough minimum was located at higher and lower latitudes than the plasmapause in the daytime and nighttime. During the main phase of the geomagnetic storms (Figure 8c), the locations of the midlatitude trough minimum and plasmapause showed a clear MLT variation. The plasmapause tended to be located at the higher and lower latitudes in the

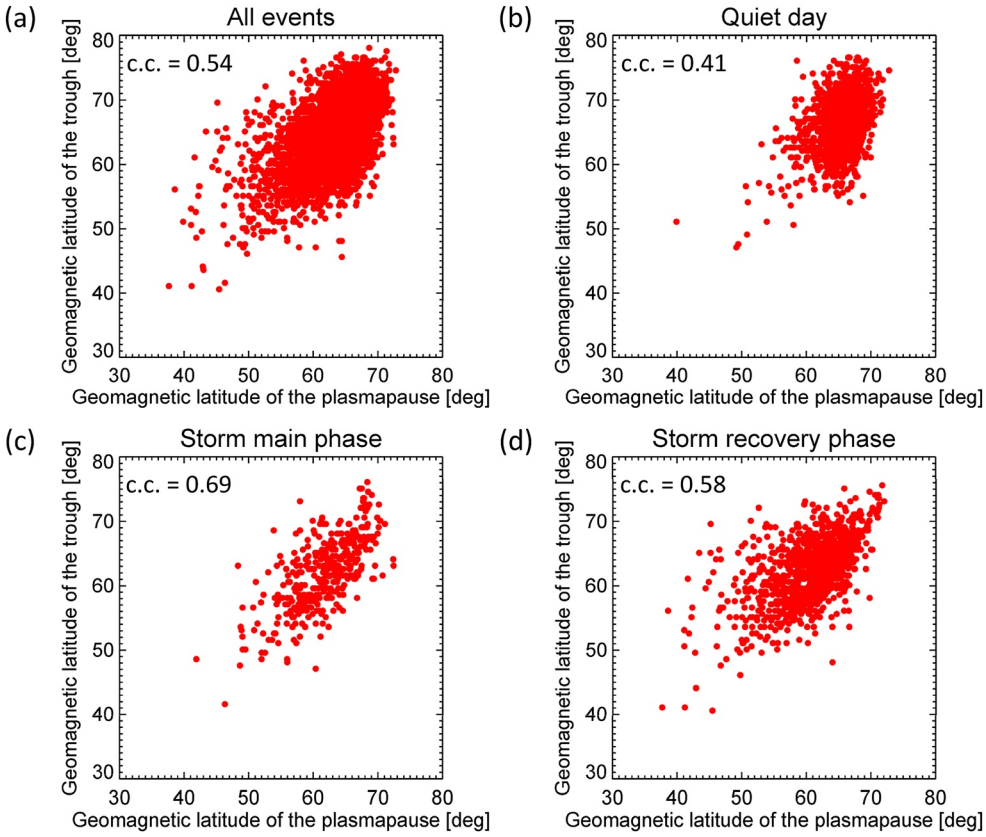

Figure 7. Correlation between the locations of the midlatitude trough minimum and plasmapause for (a) all events, (b) geomagnetically quiet days, (c) storm main phase, and (d) storm recovery phase. The correlation coefficient (c.c.) is shown on the left side of each panel.

afternoon and morning sectors. The second peak of the location of the plasmapause appeared in the dawn sector. The midlatitude trough minimum also tended to be located at the higher latitude in the afternoon sector while the location become the lowest at the postmidnight. In the afternoon to midnight sectors, both the features were located at almost the same GMLAT. During the recovery phase of the geomagnetic storms (Figure 8d), the plasmapause tended to be located at a higher latitude in the dawn and dusk sectors and at a lower latitude around 12 h (MLT). The midlatitude trough minimum tended to be located at a higher latitude in the daytime sector (6–18 h MLT). In this sector, there existed a significantly difference between the locations of the midlatitude trough minimum and plasmapause. The latitudinal difference reached approximately 5° at 12 h (MLT).

Figure 9 shows a MLT variation of the midlatitude trough minimum and plasmapause mapped on the equatorial plane in the inner magnetosphere in SM coordinates with the Tsyganenko 04 magnetic field model for (a) all events, (b) geomagnetically quiet days, (c) storm main phase, and (d) storm recovery phase. The MLT distribution of the midlatitude trough minimum and plasmapause almost reflects that at a height of 300 km in the ionosphere as shown in Figure 8. In this case, the budge structure of the plasmapause can be clearly seen in the afternoon to midnight sectors (14–24 h, MLT) during the main phase of the geomagnetic storms (Figure 9c). The structure of the midlatitude trough minimum also showed a similar shape to the plasmapause with a little difference. In the predawn sector (4–6 h, MLT), the plasmapause moved slightly to the outer region. This signature corresponded to the second peak of the plasmapause location in the predawn sector as seen in Figure 8c. In the morning to noon sectors, the midlatitude trough minimum was located at the outer region of the inner magnetosphere, compared with the plasmapause. During the recovery phase, the midlatitude trough minimum in the morning to afternoon sectors tended to be located at the outer region, compared with the plasmapause, but both the features were located at almost the same

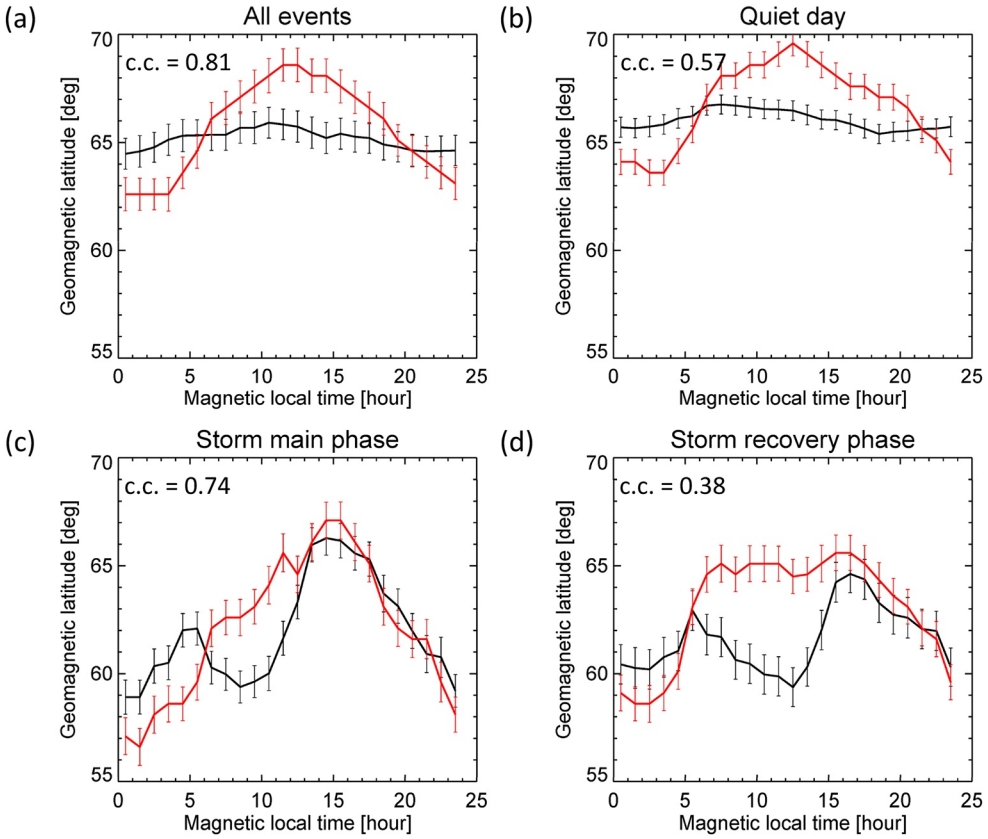

Figure 8. Magnetic local time variation of the mid-latitude trough minimum and plasmapause at a height of 300 km in the ionosphere for (a) all events, (b) geomagnetically quiet days, (c) storm main phase, and (d) storm recovery phase. The black and red lines indicate the median values of the plasmapause and midlatitude trough minimum locations every hour in the MLT window of ±1.0 h, respectively. The error bars of each curve mean the standard error of the median values. The correlation coefficient (c.c.) is shown on the left side of each panel. MLT, magnetic local time.

L-value. Furthermore, during this period, the plasmapause moved slightly to the outer region in the dawn and dusk sectors (5–6 h and 15–21 h, MLT), respectively.

5. Discussion

So far, the relationship between the locations of the midlatitude trough minimum and plasmapause has been investigated using various kinds of observation data taken by different techniques by previous studies (e.g., Chen et al., 2018; Köhnlein & Raitt, 1977; Rodger et al., 1986; Rycroft & Thomas, 1970; Smith et al., 1987; Titheridge, 1976; Yizengaw & Moldwin, 2005). Smith et al. (1987) confirmed that the plasmapause and mid-latitude trough often occurred on the same magnetic field line in the morning sector using a combination of ground whistler and ionosonde observations and that the plasmapause coincided with a poleward wall of the midlatitude trough in the evening sector. Recently, Chen et al. (2018) showed that the plasmapause tended to be located at an equatorward wall of the midlatitude trough in all geographic longitudes using lightning whistler, electron density and temperature observed by the DEMETER satellite. On the other hand, Yizengaw and Moldwin (2005) verified that the plasmapause coincided with an equatorward wall of the midlatitude trough in the afternoon sector from a comparison between the IMAGE EUV images and GPS-TEC tomography data during a super geomagnetic storm and geomagnetically quiet day. As described above, however, most of the previous studies analyzed the signature of the ELF/VLF electromagnetic waves (whistler-mode waves) for identification of the plasmapause in the equatorial inner magnetosphere. In this method, the plasmapause without in situ observation data in the equatorial magnetosphere can be identified, but the MLT and GMLAT distributions of the location of the plasmapause cannot accurately be determined due to a significant dependence of the lightning whistler activity and its propagation path.

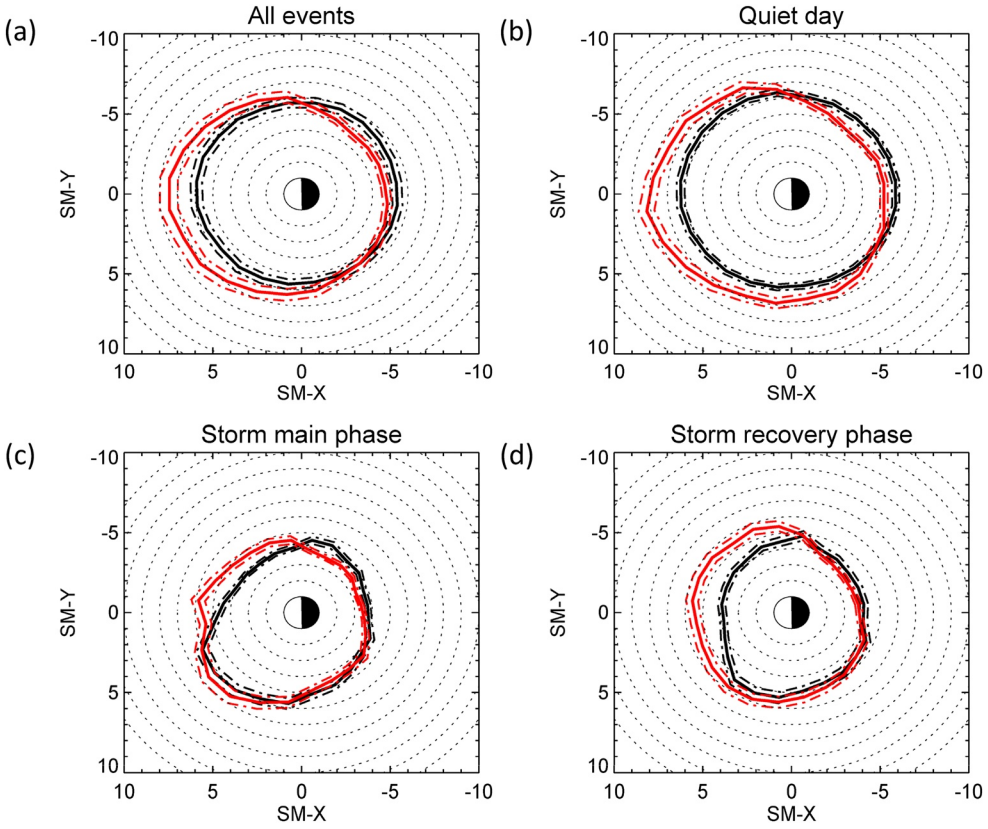

Figure 9. Magnetic local time variation of the midlatitude trough minimum and plasmapause mapped on the equatorial plane in SM coordinates for (a) all events, (b) geomagnetically quiet days, (c) storm main phase, and (d) storm recovery phase. The black and red lines indicate the median values of the plasmapause and mid-latitude trough minimum locations, respectively. The dotted-dash lines of each curve mean the width of standard error of the median values. SM, solar magnetic.

Therefore, the relationship between the locations of the midlatitude trough and plasmapause was variable by each previous study. To solve this problem, in the present study, we analyzed the simultaneous electron density data in the ionosphere and equatorial inner magnetosphere using GNSS-TEC and Arase satellite observations. As a result, the present study showed that the plasmapause is not always consistent with the location of the midlatitude trough minimum in Figures 8 and 9, and that the MLT distribution of both the features is changed significantly, depending on geomagnetic conditions (geomagnetically quiet days, main and recovery phases of the geomagnetic storms).

According to the theory of the formation of the plasmapause proposed by Nishida (1966), the plasmapause is formed at a region of counteraction of corotation and dawn-to-dusk convection electric fields in the magnetosphere. Therefore, it can be expected that the shape of the plasmapause shows strong day-night and dawn-dusk asymmetries as the convection electric field increases in association with the development of a geomagnetic storm. In fact, the present study showed that the shape of the plasmapause changes from a circle to an ellipse during a period of geomagnetic storms. From a comparison between Figures 9b and 9c, the plasmapause moved the largest distance from $L = 6.0$ to 4.0 in the morning to noon sectors (6–12 h, MLT) during the main phase of the geomagnetic storms. In the afternoon to evening sectors (15–18 h, MLT) where the bulge structure of the plasmasphere and plasmaspheric tail are formed, the location of the plasmapause was not changed significantly. On the other hand, the midlatitude trough minimum tended to be located at almost the same location as the plasmapause in the afternoon to midnight sectors (14–24 h MLT) as shown in Figures 8c and 9c. This implies that both the features are produced along the same magnetic field line between the ionosphere and inner magnetosphere. Therefore, from the above discussion, it can be expected that both the midlatitude trough and plasmapause is formed along the same magnetic field line

due to an enhancement of the large-scale convection electric field in the ionosphere and inner magnetosphere during the main phase of the geomagnetic storms. In the following discussion, we will consider the relationship between the formation of the plasmapause and midlatitude trough and storm-time electric fields (SAPS/SAID electric field, over-shielding electric field, and disturbance dynamo field).

Associated with the development of geomagnetic storms, the two-cell convection at high latitudes enhances significantly and expands to subauroral latitude and midlatitude regions (e.g., Gonzalez et al., 1994). Further, an intense westward plasma flow called a SAPS/SAID phenomenon also appears equatorward of the two-cell convection at high latitudes (e.g., Foster & Burke, 2002; Foster & Vo, 2002). From recent studies, it is shown that the SAPS/SAID westward plasma flow during the main phase of a geomagnetic storm almost coincides with the electron depletion region related to the midlatitude trough (He et al., 2018), and that the enhanced SAPS electric fields play a major role in the formation of the plasmaspheric plume and the erosion of the plasmasphere (Goldstein et al., 2005). Shinbori et al. (2005) showed that the plasmapause was formed near the enhanced electric field structure in the inner magnetosphere associated with the SAPS phenomenon during a geomagnetic storm using the Akebono satellite observation data. Actually, the present study also showed that the structure of the mid-latitude trough almost coincided with the large potential drop due to the SAPS electric field in the afternoon-midnight sectors (Figure 3e) during the main phase of a geomagnetic storm that occurred on November 7–8, 2017. The similar feature was also shown by Shinbori et al. (2020), who reported the temporal and spatial variations of TEC enhancements during a geomagnetic storm on September 27 and 28, 2017 using GNSS-TEC, SuperDARN radar, Jicamarca incoherent scatter radar, and geomagnetic field data. From the above discussion, a major reason why the location of the midlatitude trough minimum coincides with the plasmapause in the afternoon to midnight sectors is that the SAPS electric fields associated with the geomagnetic storms form both the structures on almost the same magnetic field line.

During the recovery phase of a geomagnetic storm, it has been well-known that an over-shielding electric field originating from the region-2 field-aligned currents and disturbance dynamo appears in the inner magnetosphere and midlatitude to the equatorial ionosphere (e.g., Blanc & Richmond, 1980; Fejer et al., 2008; Kikuchi et al., 2008; Shinbori et al., 2020). Fejer et al. (2008) showed that the intensity of the over-shielding electric field in the equatorial ionosphere becomes the largest in the postmidnight to predawn sectors (0–5 h, LT: local time) from a statistical analysis of the ROCSAT-1 satellite data. Because the direction of the over-shielding electric field in these sectors is opposite to that of both the convection and corotation electric fields, it can be expected that the sunward flow of the dawn plasmaspheric plasma becomes slow and the stagnation point is formed in the inner magnetosphere. Using the data-driven Magnetospheric Specification Model, Goldstein et al. (2002) reproduced the formation and subsequent evolution of the shoulder structure of the plasmapause around the dawn sector for a storm event on May 24 and 25, 2000, and they concluded that the generation of the shoulder is caused by a dusk-to-dawn over-shielding electric field due to sudden northward turning of the IMF. The present study showed that the MLT distribution of the plasmapause has the second peak of GMLT around 5 h (MLT) as seen in Figures 8c and 8d. This MLT dependence of the plasmapause is thought as the formation of the shoulder structure due to the over-shield electric field. Further, in this study, the shoulder structure was also observed during the main phase of the geomagnetic storms. This reason is that we identified the main phase of the geomagnetic storms as a period of dSYM-H/dt < 0. In this analysis method, the dSYM-H/dt < 0 events occurring during the recovery phase of the geomagnetic storm are included. To reduce the contamination of an effect of the previous storm event, we need to exclude such the events. However, because the number of geomagnetic storms is not enough to identify only the pure main phase in the present data analysis period, this point should be done in future study. On the other hand, the midlatitude trough minimum did not show an MLT distribution corresponding to the shoulder structure of the plasmapause in Figures 8c and 8d. This suggests that the MLT variation of the midlatitude trough minimum is affected not only by the over-shielding electric field but also by particle precipitation, thermospheric composition change and neutral wind in the F2-region at a lower latitude of the foot point of the region-2 field-aligned currents in the dawn sector. However, in the present data analysis, we could not identify a major reason why the midlatitude trough minimum does not reflect the shape of the shoulder in the predawn sector. These points should be solved in future study.

In the present study, the correlation between the locations of the midlatitude trough minimum and plasmapause become worse during the recovery phase of the geomagnetic storms, compared with that during the main phase (Figures 8 and 9d). As one of the reasons, a pattern of the MLT variation of the midlatitude trough minimum is different from that of the plasmapause, compared with that under other geomagnetic conditions as seen in Figures 8b–8d. Although most of the previous studies reported a geomagnetic activity dependence of the position of the midlatitude trough minimum using the *Kp* index (e.g., Chen et al., 2018), Yang et al. (2016) statistically investigated the response of the position of the midlatitude trough to the main and recovery phase of the geomagnetic storms as a function of the Dst index, and found the rapid movement of the midlatitude rough minimum to the pre-storm level after the onset of the recovery phase of the geomagnetic storms. However, Yang et al. (2016) could not investigate a change of an MLT distribution of the midlatitude trough minimum associated with a development and decay of the geomagnetic storms because they used DMSP satellite observation data for identification of the midlatitude trough minimum. According to the plasmaspheric modeling study by Wilson et al. (1993), it takes 2–3 days for the plasmasphere to recover a level of the geomagnetically quiet periods. Therefore, it can be expected that the plasmapause does not also rapidly move during the geomagnetically quiet periods. From the above discussion, we can consider that the relationship between the location of the midlatitude trough minimum and plasmapause breaks down in the daytime during the recovery phase of the geomagnetic storms.

During the geomagnetically quiet periods, it was shown that the midlatitude trough minimum appeared at a higher and lower latitude in the daytime and nighttime while the plasmapause did not almost change as a function of MLT in Figure 8b. The maximum latitudinal difference was 3.5° and 2.5° in the daytime and nighttime, respectively. From a comparison between Figures 2g–2i shown in Aa et al. (2020) and Figure 8b of the present study, the MLT behavior of the midlatitude trough minimum is basically consistent with that of the previous study but the amplitude of the latitudinal variation becomes smaller than that of Aa et al. (2020). This reason is mainly due to the difference of data sets and selections because Aa et al. (2020) analyzed the Swarm satellite data from December 2013 to November 2019 and set $Kp \leq 3$ as a quiet condition. For example, in the present statistical analysis, we deal with only the simultaneous observation of the plasmapause in the inner magnetosphere and midlatitude trough minimum in the ionosphere. On the other hand, according to Figures 4e and 4f shown in Kwon et al. (2015), the shape of the plasmapause almost was almost the circle with a radius of $L = 6.6$ during the geomagnetically quiet periods ($Kp \leq 1$). This result is almost consistent with that of Figure 9b in the present study. In this case, Kwon et al. (2015) analyzed Time History of Events and Macroscale Interactions during Substorms (THEMIS) spacecraft observation data for 2-year period (2008 and 2009), and their data set was different from that of the present study. Nevertheless, there was no significant difference of the location and shape of the mean plasmapause between both the studies. This reason may be that the analysis method to identify the plasmapause from the electron/plasma density is the same as that used in the present study. From these observational facts, it can be considered that the plasmapause is formed around $L = 6.0$ in the inner magnetosphere during the geomagnetic quiet periods. Therefore, according to the theory of Nishida (1966), the co-rotation electric field is dominant up to a large distance (at least $L = 6.0$) of the inner magnetosphere due to a significantly weak magnetospheric convection under the geomagnetically quiet condition. As a likely candidate for the generation mechanism of the midlatitude trough in the dusk to midnight sectors during the geomagnetically quiet periods, Spiro et al. (1978) proposed that the plasma density decreases significantly in a quasi-stagnation region equatorward of the auroral zone due to prolonged recombination in the dark sectors having no photoionization. They found that the location of the trough minimum appears at a 1°–2° higher latitude than that of the stagnation line corresponding to the counteraction of corotation and high-latitude convection electric fields where the plasmapause is formed in the inner magnetosphere. Nilsson et al. (2005) also concluded that the geomagnetically quiet-time midlatitude trough in the evening-midnight sectors can explain by the flow stagnation and loss process in the dark region from a comparison between the EISCAT radar observation and a simple stagnation model. Further, Nilsson et al. (2005) found that the midlatitude trough minimum is formed at a 1°–2° higher latitude of the flow stagnation line. The present study showed that the midlatitude trough minimum in the evening sector (18–21 h MLT) appears at 1°–2° higher latitude of the plasmapause which is formed at a region of counteraction of corotation and convection electric fields. The latitudinal relationship is almost consistent with the results of Spiro et al. (1978) and Nilsson et al. (2005). Therefore, this relationship between both the features at the ionospheric height may be explained by the flow

stagnation mechanism. However, because this theory cannot simply be applied for the postmidnight-dawn sector where the convection flow becomes almost the same direction as the corotation, we need to consider other generation mechanism of the midlatitude trough in the dawn sector. This point should be solved in future study using global atmosphere-ionosphere coupling model.

6. Conclusions

To clarify the relationship between the locations of the midlatitude trough minimum in the ionosphere and plasmapause in the inner magnetosphere under geomagnetically different conditions, we analyzed GNSS-TEC and electron density data obtained from the Arase satellite from March 23, 2017 to May 31, 2020. In this analysis, we identified the midlatitude trough minimum as a minimum value of GNSS-TEC at a lower latitude of the TEC enhancement associated with auroral oval, and determined the plasmapause as an electron density decrease by a factor of 5 or more within $\Delta L < 0.5$ in the inner magnetosphere according to a definition of Carpenter and Anderson (1992). As a result, we found that the location of the plasmapause does not always coincide with that of the midlatitude trough minimum in all MLT sectors during geomagnetically quiet periods, the main and recovery phases of the geomagnetic storms. During the geomagnetically quiet periods, the location of the midlatitude trough minimum showed a clear MLT variation indicating that it appeared at higher and lower latitudes in the daytime and nighttime, respectively, while the plasmapause is located at a latitude of 66° in all MLT sectors. The maximum latitudinal difference between both the features was 3.5° and 2.5° in the daytime and nighttime, respectively. This indicates that the midlatitude trough minimum and plasmapause do not always exist on the same magnetic field line. During the main phase of geomagnetic storms, the locations of the midlatitude trough minimum and plasmapause move toward a low-latitude region with day-night and dawn-dusk asymmetries. In this case, both the features were located at almost the same latitudes (or L-values) in the afternoon to dusk sectors. Further, the correlation coefficient between the locations of the midlatitude trough minimum and plasmapause becomes highest during the main phase, compared with other geomagnetic conditions. In a case study, we also showed that a SAPS electric field is distributed equatorward of the enhanced dusk convection cell and exists along the midlatitude trough structure during the main phase of a geomagnetic storm that occurred on November 7 and 8, 2017. This suggests that the formation of the midlatitude trough and erosion of the plasmasphere in the afternoon to midnight sectors occur at almost the same location due to an enhancement of convection electric field and SAPS during the main phase of geomagnetic storms. During the recovery phase of the geomagnetic storms, the locations of the midlatitude trough minimum and plasmapause showed a different MLT variation, and the latitudinal difference between both the features became larger in the daytime (6–16 h MLT). The value of the latitudinal difference became maximum around the noon. This suggests that the relationship between the location of the midlatitude trough minimum and plasmapause breaks down in the daytime during the recovery phase of the geomagnetic storms. Furthermore, the MLT variation of the location of the plasmapause showed a second peak of GMLT around 5 h (MLT). This signature in the dawn sector corresponds to the shoulder structure of the plasmasphere produced by the over-shielding electric fields associated with the dominance of the region-2 field-aligned current system. This feature was observed during both the main and recovery phases of the geomagnetic storms.

Data Availability Statement

The solar wind and IMF data were provided by provided by the National Aeronautics and Space Administration (NASA) Coordinated Data Analysis Web (CDAWeb) (https://cdaweb.sci.gsfc.nasa.gov/index.html/). The authors used geomagnetic indices (AE and SYM-H) with 1-min time resolution provided by the World Data Center (WDC) for Geomagnetism, Kyoto University (http://wdc.kugi.kyoto-u.ac.jp/index.html). The authors also referred to a list of geomagnetically quiet and disturbed days provided by the GFZ German Research Centre for Geosciences (https://www.gfz-potsdam.de/en/kp-index/). The Receiver Independent Exchange Format (RINEX) data used for GNSS-TEC processing were provided by 50 data providers. These have been listed on the webpage of the GNSS-TEC database (http://stdb2.isee.nagoya-u.ac.jp/GPS/GPS-TEC/gnss_provider_list.html). The mainly contributed providers are UNAVCO (https://www.unavco.org/data/gps-gnss/gps-gnss.html), CDDIS (https://cddis.nasa.gov/archive/gnss/data/daily/, Noll, 2010), CHAIN (http://chain.physics.unb.ca/chain/pages/data_download, Jayachandran et al., 2009), PNGA (http://www.

geodesy.cwu.edu, Pacific Northwest Geodetic Array (PANGA), 1996), IBGE (http://geoftp.ibge.gov.br/informacoes_sobre_posicionamento_geodesico/rbmc/dados/), SOPAC (http://garner.ucsd.edu/pub/rinex/), GEONET (http://datahouse1.gsi.go.jp/terras/terras_english.html), GNNZ (https://www.geonet.org.nz/data/types/geodetic), RENAG (https://doi.org/10.15778/resif.rg, RESIF, 2017), SONEL (https://www.sonel.org/-GPS-.html), LINZ (https://apps.linz.govt.nz/ftp/positionz), INGV (http://ring.gm.ingv.it/, INGV RING Working Group, 2016), SWSBM (https://www.sws.bom.gov.au/World_Data_Centre/1/1), AFREF (http://afrefdata.org/), TLALOCNET (http://tlalocnet.udg.mx/tlalocnetgsac/), NCEDC (https://ncedc.org/bard.overview.html, NCEDC, 2014), EUREF (https://www.epncb.oma.be/, Bruyninx et al., 2019), RAMSAC (https://www.ign.gob.ar/NuestrasActividades/Geodesia/Ramsac/DescargaRinex, Pinon et al., 2018), and BIGF (http://www.bigf.ac.uk/data_access.html). Science data of the ERG (Arase) satellite were obtained from the ERG Science Center operated by ISAS/JAXA and ISEE/Nagoya University (https://ergsc.isee.nagoya-u.ac.jp/index.shtml.en, Miyoshi, Hori, et al., 2018). The present study used PWE/HFA L2 v01_01 (Kasahara, Kumamoto, et al., 2018), PWE/HFA L3 v01_02 (Kasahara et al., 2021), MGF-L2 v03_03 (Matsuoka, Teramoto, Imajo, et al., 2018), OBT L2 v03 (Miyoshi et al., 2018a), and OBT L3 v02 (Miyoshi et al., 2018b) data. The SuperDARN electric potential map data and analysis software were provided by Virginia Tech (http://vt.superdarn.org/tiki-index.php?page=ASCIIData).

Acknowledgments
This study was supported by a JSPS KAKENHI Grant numbers 26400478 and 16H06286 and the National Institute of Polar Research (NIPR) through General Collaboration Project no. 29-11. The coauthor (Yuichi Otsuka) was also supported by a MEXT/JSPS KAKENHI Grant numbers 15H05815 and 16H05736. The authors used the Inter-university Upper atmosphere Global Observation NETwork (IUGONET) database (IUGONET Type-A) and data analysis software (UDAS). The GNSS data collection and processing were performed using the NICT Science Cloud. SuperDARN is a collection of radars funded by the national scientific funding agencies of Australia, Canada, China, France, Italy, Japan, Norway, South Africa, United Kingdom, and the United States.

References

Aa, E., Zou, S., Erickson, P. J., Zhang, S. R., & Liu, S. (2020). Statistical analysis of the main ionospheric trough using Swarm in situ measurements. *Journal of Geophysical Research: Space Physics*, *125*, e2019JA027583. https://doi.org/10.1029/2019JA027583

Afonin, V. V., Benkova, N. P., Besprozvannaya, A. S., Shchuka, T. I., Zikrach, E. K., & Shestakova, L. V. (1995). The ionospheric trough dynamics in the Northern and Southern Hemispheres: The longitudinal and IMF effect. *Journal of Atmospheric and Terrestrial Physics*, *57*, 1057–1062. https://doi.org/10.1016/0021-9169(95)96865-T

Ahmed, M., Sagalyn, R. C., Wildman, P. J. L., & Burke, W. J. (1979). Topside ionospheric trough morphology: Occurrence frequency and diurnal, seasonal, and altitude variations. *Journal of Geophysical Research*, *84*, 489–498. https://doi.org/10.1029/JA084iA02p00489

Anderson, P. C., Heelis, R. A., & Hanson, W. B. (1991). The ionospheric signatures of rapid subauroral ion drifts. *Journal of Geophysical Research*, *96*, 5785–5792. https://doi.org/10.1029/90JA02651

Angelopoulos, V., Cruce, P., Drozdov, A., Grimes, E. W., Hatzigeorgiu, N., King, D. A., et al. (2019). The Space Physics Environment Data Analysis System (SPEDAS). *Space Science Reviews*, *215*. https://doi.org/10.1007/s11214-018-0576-4

Blanc, M., & Richmond, A. D. (1980). The ionospheric disturbance dynamo. *Journal of Geophysical Research*, *85*, 1669–1686. https://doi.org/10.1029/JA085iA04p01669

Bruyninx, C., Legrand, J., Fabian, A., & Pottiaux, E. (2019). GNSS metadata and data validation in the EUREF Permanent Network. *GPS Solutions*, *23*, 106. https://doi.org/10.1007/s10291-019-0880-9

Carpenter, D. L. (1966). Whistler studies of the plasmapause in the magnetosphere: 1. Temporal variations in the position of the knee and some evidence on plasma motions near the knee. *Journal of Geophysical Research*, *71*, 693–709. https://doi.org/10.1029/JZ071i003p00693

Carpenter, D. L., & Anderson, R. R. (1992). An ISEE/whistler model of equatorial electron density in the magnetosphere. *Journal of Geophysical Research*, *97*, 1097–1108. https://doi.org/10.1029/91JA01548

Chappell, C. R. (1975). Ionosphere-magnetosphere coupling: 1. Thermal plasma. *Reviews of Geophysics*, *13*, 872–873. https://doi.org/10.1029/RG013i003p00872

Chappell, C. R., Harris, K. K., & Sharp, G. W. (1970). A study of the influence of magnetic activity on the location of the plasmapause as measured by OGO 5. *Journal of Geophysical Research*, *75*, 50–56. https://doi.org/10.1029/JA075i001p00050

Chen, C. Y., Liu, T. J. Y., Lee, I. T., Rothkaehl, H., Przepiorka, D., Chang, L. C., et al. (2018). The midlatitude trough and the plasmapause in the nighttime ionosphere simultaneously observed by DEMETER during 2006-2009. *Journal of Geophysical Research: Space Physics*, *123*, 5917–5932. https://doi.org/10.1029/2017JA024840

Coster, A. J., Erickson, P. J., Foster, J. C., Thomas, E. G., Ruohoniemi, J. M., & Baker, J. (2017). Solar cycle 24 observations of storm-enhanced density and the tongue of ionization. In T. Fuller-Rowell, E. Yizengaw, P. H. Doherty, & S. Basu, (Eds.), *Ionospheric space weather: Longitude and hemispheric dependences and lower atmosphere forcing, Geophysical Monograph* (Vol. 220, pp. 71–83). American Geophysical Union.

Cousins, E. D. P., Matsuo, T., & Richmond, A. D. (2013). SuperDARN assimilative mapping. *Journal of Geophysical Research: Space Physics*, *118*, 7954–7962. https://doi.org/10.1002/2013JA019319

Dudeney, J. R., Rodger, A. S., & Jarvis, M. J. (1983). Radio studies of the main F region trough in Antarctica. *Radio Science*, *18*, 927–936. https://doi.org/10.1029/RS018i006p00927

Fejer, B. G., Jensen, J. W., & Su, S.-Y. (2008). Seasonal and longitudinal dependence of equatorial disturbance vertical plasma drifts. *Geophysical Research Letters*, *35*. https://doi.org/10.1029/2008GL035584

Foster, J. C., & Burke, W. J. (2002). SAPS: A new categorization for sub-auroral electric fields. *Eos, Transactions American Geophysical Union*, *83*, 393. https://doi.org/10.1029/2002EO000289

Foster, J. C., Coster, A. J., Erickson, P. J., Goldstein, J., & Rich, F. J. (2002). Ionospheric signatures of plasmaspheric tails. *Geophysical Research Letters*, *29*, 1623. https://doi.org/10.1029/2002GL015067

Foster, J. C., & Vo, H. B. (2002). Average characteristics and activity dependence of the subauroral polarization stream. *Journal of Geophysical Research*, *107*, 16. https://doi.org/10.1029/2002JA009409

Goldstein, J. (2004). Simultaneous remote sensing and in situ observations of plasmaspheric drainage plumes. *Journal of Geophysical Research*, *109*, A03202. https://doi.org/10.1029/2003JA010281

Goldstein, J. (2006). Plasmasphere response: Tutorial and review of recent imaging results. *Space Science Reviews*, *124*, 203–216. https://doi.org/10.1007/s11214-006-9105-y

Goldstein, J., Sandel, B. R., Forrester, W. T., Thomsen, M. F., & Hairston, M. R. (2005). Global plasmasphere evolution 22-23 April 2001. *Journal of Geophysical Research*, *110*, A12218. https://doi.org/10.1029/2005JA011282

Goldstein, J., Spiro, R. W., Reiff, P. H., Wolf, R. A., Sandel, B. R., Freeman, J. W., & Lambour, R. L. (2002). IMF-driven overshielding electric field and the origin of the plasmaspheric shoulder of May 24, 2000. *Geophysical Research Letters*, *29*, 66. https://doi.org/10.1029/2001GL014534

Gonzalez, W. D., Joselyn, J. A., Kamide, Y., Kroehl, H. W., Rostoker, G., Tsurutani, B. T., & Vasyliunas, V. M. (1994). What is a geomagnetic storm? *Journal of Geophysical Research*, *99*, 5771–5792. https://doi.org/10.1029/93JA02867

Hayashi, H., Koyama, Y., Hori, T., Tanaka, Y., Abe, S., Shinbori, A., et al. (2013). Inter-university Upper Atmosphere Global Observation NETwork (IUGONET). *Data Science Journal*, *12*, WDS179–WDS184. https://doi.org/10.2481/dsj.WDS-030

He, F., Zhang, X.-X., Wang, W., Liu, L., Ren, Z.-P., Yue, X., et al. (2018). Large-scale structure of subauroral polarization streams during the main phase of a severe geomagnetic storm. *Journal of Geophysical Research: Space Physics*, *123*, 2964–2973. https://doi.org/10.1002/2018JA025234

Heber, B., Sanderson, T. R., & Zhang, M. (1999). Corotating interaction regions. *Advances in Space Research*, *23*, 567–579. https://doi.org/10.1016/S0273-1177(99)80013-1

Hedin, M., Haggstrom, I., Pellinen-Wannberg, A., Andersson, L., Brandstrom, U., Gustavasson, B., et al. (2000). 3-D extent of the main ionospheric trough – A case study. *Advances in Polymer Atmospheric Research*, *14*, 157–162.

Holt, J. M., Evans, J. V., & Wand, R. H. (1983). Millstone Hill studies of the trough: Boundary between the plasmapause and magnetosphere or not? *Radio Science*, *18*, 947–954. https://doi.org/10.1029/RS018i006p00947

INGV RING Working Group. (2016). *Rete Integrata Nazionale GNSS*. https://doi.org/10.13127/RING

Ishida, T., Ogawa, Y., Kadokura, A., Hiraki, Y., & Häggström, I. (2014). Seasonal variation and solar activity dependence of the quiet-time ionospheric trough. *Journal of Geophysical Research: Space Physics*, *119*, 6774–6783. https://doi.org/10.1002/2014JA019996

Iyemori, T. (1990). Storm-time magnetospheric currents inferred from mid-latitude geomagnetic field variations. *Journal of Geomagnetism and Geoelectricity*, *42*, 1249–1265. https://doi.org/10.5636/jgg.42.1249

Iyemori, T., & Rao, D. R. K. (1996). Decay of the Dst field of geomagnetic disturbance after substorm onset and its implication to storm-substorm relation. *Annales Geophysicae*, *14*, 608–618. https://doi.org/10.1007/s00585-996-0608-3

Jayachandran, P. T., Langley, R. B., MacDougall, J. W., Mushini, S. C., Pokhotelov, D., Hamza, A. M., et al. (2009). Canadian High Arctic Ionospheric Network (CHAIN). *Radio Science*, *44*. https://doi.org/10.1029/2008RS004046

Karpachev, A. T., Klimenko, M. V., & Klimenko, V. V. (2019). Longitudinal variations of the ionospheric trough position. *Advances in Space Research*, *63*, 950–966. https://doi.org/10.1016/j.asr.2018.09.038

Kasahara, Y., Kasaba, Y., Kojima, H., Yagitani, S., Ishisaka, K., Kumamoto, A., et al. (2018). The Plasma Wave Experiment (PWE) on board the Arase (ERG) Satellite. *Earth Planets and Space*, *70*, 86. https://doi.org/10.1186/s40623-018-0842-4

Kasahara, Y., Kumamoto, A., Tsuchiya, F., Kojima, H., Matsuda, S., Matsuoka, A., et al. (2021). *The PWE/HFA instrument Level-3 electron density data of Exploration of energization and Radiation in Geospace (ERG) Arase satellite*. https://doi.org/10.34515/DATA.ERG-10001

Kasahara, Y., Kumamoto, A., Tsuchiya, F., Matsuda, S., Shoji, M., Nakamura, S., et al. (2018). *The PWE/HFA instrument Level-2 spectrum data of Exploration of energization and Radiation in Geospace (ERG) Arase satellite*. https://doi.org/10.34515/DATA.ERG-10000

Kelley, M. (2009). *The Earth's ionosphere: Plasma physics and electrodynamics* (2nd ed.). California Academic Press.

Kersley, L., Pryse, S. E., Walker, I. K., Heaton, J. A. T., Mitchell, C. N., Williams, M. J., & Willson, C. A. (1997). Imaging of electron density troughs by tomographic techniques. *Radio Science*, *32*, 1607–1621. https://doi.org/10.1029/97RS00310

Kikuchi, T., Hashimoto, K. K., & Nozaki, K. (2008). Penetration of magnetospheric electric fields to the equator during a geomagnetic storm. *Journal of Geophysical Research*, *113*. https://doi.org/10.1029/2007JA012628

Köhnlein, W., & Raitt, W. J. (1977). Position of the mid-latitude trough in the topside ionosphere as deduced from ESRO 4 observations. *Planetary and Space Science*, *25*, 600–602. https://doi.org/10.1016/0032-0633(77)90069-1

Krankowski, A., Shagimuratov, I. I., Ephishov, I. I., Krypiak-Gregorczyk, A., & Yakimova, G. (2009). The occurrence of the mid-latitude ionospheric trough in GPS-TEC measurements. *Advances in Space Research*, *43*, 1721–1731. https://doi.org/10.1016/j/asr.2008.05.014

Kumamoto, A., Tsuchiya, F., Kasahara, Y., Kasaba, Y., Kojima, H., Yagitani, S., et al. (2018). High Frequency Analyzer (HFA) of Plasma Wave Experiment (PWE) onboard the Arase spacecraft. *Earth Planets and Space*, *70*, 82. https://doi.org/10.1186/s40623-018-0854-0

Kwon, H. J., Kim, K. H., Jee, G., Park, J. S., Jin, H., & Nishimura, Y. (2015). Plasmapause location under quiet geomagnetic conditions (Kp ≤ 1): THEMIS observations. *Geophysical Research Letters*, *42*, 7303–7310. https://doi.org/10.1002/2015GL066090

Matsuoka, A., Teramoto, M., Imajo, S., Kurita, S., Miyoshi, Y., & Shinohara, I. (2018). The *MGF instrument Level-2 high-resolution magnetic field data of Exploration of energization and Radiation in Geospace (ERG) Arase satellite*. https://doi.org/10.34515/DATA.ERG-06000

Matsuoka, A., Teramoto, M., Nomura, R., Nosé, M., Fujimoto, A., Tanaka, Y., et al. (2018). The ARASE (ERG) magnetic field investigation. *Earth Planets and Space*, *70*, 43. https://doi.org/10.1186/s40623-018-0800-1

Miyoshi, Y., Hori, T., Shoji, M., Teramoto, M., Chang, T. F., Segawa, T., et al. (2018). The ERG Science Center. *Earth Planets and Space*, *70*, 96. https://doi.org/10.1186/s40623-018-0867-8

Miyoshi, Y., Shinohara, I., & Jun, C.-W. (2018a). *The Level-2 orbit data of Exploration of energization and Radiation in Geospace (ERG) Arase satellite*. https://doi.org/10.34515/DATA.ERG-12000

Miyoshi, Y., Shinohara, I., & Jun, C.-W. (2018b). T*he Level-3 orbit data of Exploration of energization and Radiation in Geospace (ERG) Arase satellite*. https://doi.org/10.34515/DATA.ERG-12001

Miyoshi, Y., Shinohara, I., Takashima, T., Asamura, K., Higashio, N., Mitani, T., et al. (2018). Geospace Exploration Project ERG. *Earth Planets and Space*, *70*, 101. https://doi.org/10.1186/s40623-018-0862-0

Moldwin, M. B., Zou, S., & Heine, T. (2016). The story of plumes: The development of a new conceptual framework for understanding magnetosphere and ionosphere coupling. *Annales Geophysicae*, *34*, 1243–1253. https://doi.org/10.5194/angeo-34-1243-2016

Muldrew, D. B. (1965). F-layer ionization troughs deduced from Alouette data. *Journal of Geophysical Research*, *70*, 2635–2650. https://doi.org/10.1029/JZ070i011p02635

NCEDC. (2014). *Northern California Earthquake data center*. UC Berkeley Seismological Laboratory. Dataset. https://doi.org/10.7932/NCEDC

Nilsson, H., Sergienko, T. I., Ebihara, Y., & Yamauchi, M. (2005). Quiet-time mid-latitude trough: Influence of convection, field-aligned currents and proton precipitation. *Annales Geophysicae*, *23*, 3277–3288. https://doi.org/10.5194/angeo-23-3277-2005

Nishida, A. (1966). Formation of plasmapause, or magnetospheric plasma knee, by the combined action of magnetospheric convection and plasma escape from the tail. *Journal of Geophysical Research*, *71*, 5669–5679. https://doi.org/10.1029/JZ071i023p05669

Nishitani, N., Ruohoniemi, J. M., Lester, M., Baker, J. B. H., Koustov, A. V., Shepherd, S. G., et al. (2019). Review of the accomplishments of mid-latitude Super Dual Auroral Radar Network (SuperDARN) HF radars. *Progress in Earth and Planetary Science*, *6*, 27. https://doi.org/10.1186/s40645-019-0270-5

Noll, C. E. (2010). The Crustal Dynamics Data Information System: A resource to support scientific analysis using space geodesy. *Advances in Space Research*, *45*, 1421–1440. https://doi.org/10.1016/j.asr.2010.01.018

Ober, D. M., Horwitz, J. L., Thomsen, M. F., Elphic, R. C., McComas, D. J., Belian, R. D., & Moldwin, M. B. (1997). Premidnight plasmaspheric "plumes". *Journal of Geophysical Research*, *102*, 11325–11334. https://doi.org/10.1029/97JA00562

Otsuka, Y., Ogawa, T., Saito, A., Tsugawa, T., Fukao, S., & Miyazaki, S. (2002). A new technique for mapping of total electron content using GPS network in Japan. *Earth Planet and Space*, *54*, 63–70. https://doi.org/10.1186/bf03352422

Oya, H., & Ono, T. (1987). Stimulation of plasma waves in the magnetosphere using satellite JIKIKEN (EXOS-B). Part II. Plasma Density across the plasmapause. *Journal of Geomagnetism and Geoelectricity*, *39*, 591–607. https://doi.org/10.5636/jgg.39.591

Pacific Northwest Geodetic Array (PANGA). (1996). GPS/GNSS Network and Geodesy Laboratory: Central Washington University, other/seismic network. *International Federation of Digital Seismograph Networks*. https://doi.org/10.7914/SN/PW

Piñón, D. A., Gómez, D. D., Smalley, R., Cimbaro, S. R., Lauría, E. A., & Bevis, M. G. (2018). The history, state, and future of the Argentine continuous satellite monitoring network and its contributions to geodesy in Latin America. *Seismological Research Letters*, *89*, 475–482. https://doi.org/10.1785/0220170162

Prölss, G. W. (2007). The equatorward wall of the subauroral trough in the afternoon/evening sector. *Annales Geophysicae*, *25*, 645–659. https://doi.org/10.5194/angeo-25-645-2007

Pryse, S. E., Kersley, L., Williams, M. J., & Walker, I. K. (1998). The spatial structure of the dayside ionospheric trough. *Annales Geophysicae*, *16*, 1169–1179. https://doi.org/10.1007/s00585-998-1169-4

RESIF. (2017). *RESIF-RENAG French national Geodetic Network. RESIF - Reseau Sismologique et geodesique Francais*. https://doi.org/10.15778/resif.rg

Rodger, A. S. (2008). *The Mid-latitude trough—Revisited, Geophysical Monograph Series* (Vol. 181, pp. 25–33). American Geophysical Union. https://doi.org/10.1029/181GM04

Rodger, A. S., Brace, L. H., Hoegy, W. R., & Winningham, J. D. (1986). The poleward edge of the mid-latitude trough-its formation, orientation and dynamics. *Journal of Atmospheric and Terrestrial Physics*, *48*, 715–728. https://doi.org/10.1016/0021-9169(86)90021-8

Rodger, A. S., Moffett, R. J., & Quegan, S. (1992). The role of ion drift in the formation of ionisation troughs in the mid- and high-latitude ionosphere—A review. *Journal of Atmospheric and Terrestrial Physics*, *54*, 1–30. https://doi.org/10.1016/0021-9169(92)90082-V

Rodger, A. S., & Pinnock, M. (1982). Movements of the mid-latitude ionospheric trough. *Journal of Atmospheric and Terrestrial Physics*, *44*, 985–992. https://doi.org/10.1016/0021-9169(82)90063-0

Rothkaehl, H., Stanislawska, I., Leitinger, R., & Tulunay, Y. (2000). Application of a trough model for telecommunication purposes. *Physics and Chemistry of the Earth - C: Solar, Terrestrial & Planetary Science*, *25*, 315–318. https://doi.org/10.1016/S1464-1917(00)00024-6

Rycroft, M. J., & Burnell, S. J. (1970). Statistical analysis of movements of the ionospheric trough and the plasmapause. *Journal of Geophysical Research*, *75*, 5600–5604. https://doi.org/10.1029/JA075i028p05600

Rycroft, M. J., & Thomas, J. O. (1970). The magnetospheric plasmapause and the electron density trough at the Alouette 1 orbit. *Planetary and Space Science*, *18*, 65–80. https://doi.org/10.1016/0032-0633(70)90067-X

Sandel, B. R., Goldstein, J., Gallagher, D. L., & Spasojevic, M. (2003). Extreme Ultraviolet Imager observations of the structure and dynamics of the plasmasphere. *Space Science Reviews*, *109*, 25–46. https://doi.org/10.1023/B:SPAC.000000751.47727.5b

Schunk, R. W., Banks, P. M., & Raitt, W. J. (1976). Effects of electric fields and other processes upon the nighttime high-latitude F layer. *Journal of Geophysical Research*, *81*, 3271. https://doi.org/10.1029/JA081i019p03271

Shepherd, S. G. (2014). Altitude-adjusted corrected geomagnetic coordinates: Definition and functional approximations. *Journal of Geophysical Research: Space Physics*, *119*, 7501–7521. https://doi.org/10.1002/2014JA020264

Shinbori, A., Nishimura, Y., Ono, T., Kumamoto, A., Oya, H., & Oya, H. (2005). Electrodynamics in the duskside inner magnetosphere and plasmasphere during a super magnetic storm on March 13-15, 1989. *Earth Planet and Space*, *57*, 643–659. https://doi.org/10.1186/BF03351843

Shinbori, A., Otsuka, Y., Sori, T., Tsugawa, T., & Nishioka, M. (2020). Temporal and spatial variations of total electron content enhancements during a geomagnetic storm on 27 and 28 September 2017. *Journal of Geophysical Research: Space Physics*, *125*, e2019JA026873. https://doi.org/10.1029/2019JA026873

Shinbori, A., Otsuka, Y., Tsugawa, T., Nishioka, M., Kumamoto, A., Tsuchiya, F., et al. (2018). Temporal and spatial variations of storm time midlatitude ionospheric trough based on global GNSS-TEC and Arase satellite observations. *Geophysical Research Letters*, *45*, 7362–7370. https://doi.org/10.1029/2018GL078723

Shiokawa, K., Katoh, Y., Hamaguchi, Y., Yamamoto, Y., Adachi, T., Ozaki, M., et al. (2017). Ground-based instruments of the PWING project to investigate dynamics of the inner magnetosphere at subauroral latitudes as a part of the ERG-ground coordinated observation network. *Earth Planets and Space*, *69*, 160. https://doi.org/10.1186/s40623-017-0745-9

Smith, A. J., Rodger, A. S., & Thomas, D. W. P. (1987). Simultaneous ground-based observations of the plasmapause and the F-region mid-latitude trough. *Journal of Atmospheric and Terrestrial Physics*, *49*, 43–47. https://doi.org/10.1016/0021-9169(87)90080-8

Sori, T., Shinbori, A., Otsuka, Y., Tsugawa, T., & Nishioka, M. (2019). Characteristics of GNSS total electron content enhancements over the midlatitudes during a geomagnetic storm on 7 and 8 November 2004. *Journal of Geophysical Research: Space Physics*, *124*, 10376. https://doi.org/10.1029/2019JA026713

Spiro, R. W., Heelis, R. A., & Hanson, W. B. (1978). Ion convection and the formation of the mid-latitude F-region ionization trough. *Journal of Geophysical Research*, *83*, 4255–4264. https://doi.org/10.1029/JA083iA09p04255

Spiro, R. W., Heelis, R. A., & Hanson, W. B. (1979). Rapid subauroral ion drifts observed by Atmosphere Explorer C. *Geophysical Research Letters*, *6*, 657–660. https://doi.org/10.1029/GL006i008p00657

Tanaka, Y., Shinbori, A., Hori, T., Koyama, Y., Abe, S., Umemura, N., et al. (2013). Analysis software for upper atmospheric data developed by the IUGONET project and its application to polar science. *Advances in Polar Science*, *24*, 231–240. https://doi.org/10.3724/SP.J.1085.2013.00231

Titheridge, J. E. (1976). Plasmapause effects in the top side ionosphere. *Journal of Geophysical Research*, *81*, 3227–3233. https://doi.org/10.1029/JA081i019p03227

Tsyganenko, N. A., & Sitnov, M. I. (2005). Modeling the dynamics of the inner magnetosphere during strong geomagnetic storms. *Journal of Geophysical Research*, *110*. https://doi.org/10.1029/2004JA010798

Voiculescu, M., Virtanen, I., & Nygrén, T. (2006). The F-region trough: Seasonal morphology and relation to interplanetary magnetic field. *Annales Geophysicae*, *24*, 173–185. https://doi.org/10.1002/2016JA023360

Werner, S., & Prölss, G. W. (1997). The position of the ionospheric trough as a function of local time and magnetic activity. *Advances in Space Research*, *20*, 1717–1722. https://doi.org/10.1016/s0273-1177(97)00578-4

Whalen, J. A. (1989). The daytime F-layer trough and its relation to ionospheric-magnetospheric convection. *Journal of Geophysical Research*, *94*, 17169–17184. https://doi.org/10.1029/JA094iA12p17169

Wilson, G. R., Horwitz, J. L., & Lin, J. (1993). Semikinetic modeling of plasma flow on outer plasmaspheric field lines. *Advances in Space Research*, *13*, 107–116. https://doi.org/10.1016/0273-1177(93)90320-b

World Data Center for Geomagnetism, Kyoto, Nose, M., Iyemori, T., Sugiura, M., & Kamei, T. (2015). *Geomagnetic AE Index*. https://doi.org/10.17593/15031-54800

Yang, N., Le, H., & Liu, L. (2015). Statistical analysis of ionospheric mid-latitude trough over the Northern Hemisphere derived from GPS total electron content data. *Earth Planet and Space*, *67*, 196. https://doi.org/10.1186/s40623-015-0365-1

Yang, N., Le, H., & Liu, L. (2016). Statistical analysis of the mid-latitude trough position during different categories of magnetic storms and different storm intensities. *Earth Planets and Space*, *68*, 171. https://doi.org/10.1186/s40623-016-0554-6

Yang, N., Le, H., Liu, L., & Zhang, R. (2018). Statistical behavior of the longitudinal variations of the evening topside mid-latitude trough position in both Northern and Southern Hemispheres. *Journal of Geophysical Research: Space Physics*, *123*, 3983–3997. https://doi.org/10.1029/2017JA025048

Yizengaw, E., & Moldwin, M. (2005). The altitude extension of the mid-latitude trough and its correlation with plasmapause position. *Geophysical Research Letters*, *32*, L09105. https://doi.org/10.1029/2005GL022854

Yizengaw, E., Wei, H., Moldwin, M. B., Galvan, D., Mandrake, L., Mannucci, A., & Pi, X. (2005). The correlation between mid-latitude trough and the plasmapause. *Geophysical Research Letters*, *32*, L10102. https://doi.org/10.1029/2005GL022954

Zou, S., Moldwin, M. B., Coster, A., Lyons, L. R., & Nicolls, M. J. (2011). GPS TEC observations of dynamics of the mid-latitude trough during substorms. *Geophysical Research Letters*, *38*, L14109. https://doi.org/10.1029/2011GL048178

Zou, S., Moldwin, M. B., Nicolls, M. J., Ridley, A. J., Coster, A. J., Yizengaw, E., et al. (2013). Electrodynamics of the high-latitude trough: Its relationship with convection flows and field-aligned currents. *Journal of Geophysical Research: Space Physics*, *118*, 2565–2572. https://doi.org/10.1002/jgra.50120